A single MIU motif of MINDY-1 recognizes K48-linked polyubiquitin chains

Kristariyanto, Yosua; Rehman, Syed Arif Abdul; Weidlich, Simone; Knebel, Axel; Kulathu, Yogesh

Published in:
EMBO Reports

DOI:
10.15252/embr.201643205

Publication date:
2017

Document Version
Peer reviewed version

A single MIU motif of MINDY-1 recognizes K48-linked polyubiquitin chains

Yosua Adi Kristariyanto, Syed Arif Abdul Rehman, Simone Weidlich, Axel Knebel and Yogesh Kulathu[#]

MRC Protein Phosphorylation and Ubiquitylation Unit, College of Life Sciences, University of Dundee, Dow Street, Dundee DD1 5EH, UK

#Correspondence should be addressed to Yogesh Kulathu, MRC Protein Phosphorylation and Ubiquitylation Unit, College of Life Sciences, University of Dundee, Dow Street, Dundee DD1 5EH, UK. Email: ykulathu@dundee.ac.uk, Tel: +44 1382 388163, Fax: +44 1382 223778

Running title: Polyubiquitin recognition by the MIU motifs of MINDY-1

Key words: polyubiquitin, ubiquitin binding domain (UBD), ubiquitin signaling, motif interacting with ubiquitin (MIU), MINDY deubiquitinase

Abstract

The eight different types of ubiquitin (Ub) chains that can be formed play important roles in diverse cellular processes. Linkage-selective recognition of Ub chains by Ub-binding domain (UBD)-containing proteins is central to coupling different Ub signals to specific cellular responses. The motif interacting with ubiquitin (MIU) is a small UBD that has been characterized for its binding to monoUb. The recently discovered deubiquitinase MINDY-1/FAM63A contains a tandem MIU repeat (tMIU) that is highly selective at binding to K48-linked polyUb. We here identify that this linkage-selective binding is mediated by a single MIU motif (MIU2) in MINDY-1. The crystal structure of MIU2 in complex with K48-linked polyubiquitin chains reveals that MIU2 on its own binds to all three Ub moieties in an open conformation that can only be accommodated by K48-linked triUb. The weak Ub binder MIU1 increases overall affinity of the tMIU for polyUb chains without affecting its linkage selectivity. Our analyses reveal new concepts for linkage selectivity and polyUb recognition by UBDs.

Introduction

Ubiquitylation is a protein modification that regulates a plethora of cellular signaling [1-4]. The 76-residue ubiquitin (Ub) is attached to Lys residues of target substrates through an enzymatic cascade that involves Ub-activating enzyme (E1), Ub-conjugating enzyme (E2) and Ub-ligating enzyme (E3) [5]. Ub itself has seven Lys residues and an N-terminal Met residue that can be ubiquitylated, which results in the formation of eight types of polyubiquitin (polyUb) chains: M1, K6, K11, K27, K29, K33, K48 and K63 [6]. The different chain types are associated with different cellular functions and they adopt distinct conformations. For example, K48-linked polyUb chains that target proteins for proteasomal degradation adopt compact conformations [7]. Indeed, K48-linked polyUb chains have also been observed in open conformations, reflecting the flexible nature of polyUb chains [8,9]. Proteins containing Ub-binding domains (UBDs) recognize these distinct conformations of polyUb chains and translate the different Ub signals to produce distinct outcomes [10]. Since Ub signals regulate diverse cellular processes, they have to be removed and regulated, and this function is mainly performed by dedicated proteases called deubiquitinating enzymes (DUBs) [11].

To date, there are 21 families of UBDs reported, which vary in size, structure, and mode of binding with Ub [10,12]. Ub-interacting motif (UIM) and motif interacting with Ub (MIU)

are the smallest among the UBDs. Both motifs form an α-helical structure composed of ~20 residues [13-16]. They bind to monoUb through hydrophobic residues centered on a key alanine that interacts with the hydrophobic I44 patch (L8, I44, H68 and V70) on Ub. The signature motif of the MIU is the inverse of a UIM, which explains why monoUb binds MIU in a reverse orientation than when bound to UIM [15,16].

The affinity of a UIM for monoUb is relatively weak with dissociation constants (K_d) in the range of 100 μM to 2 mM [17]. The MIU of Rabex-5 has slightly higher affinity for monoUb at approximately 30 μM [15,16]. To compensate for the weak affinities, many proteins contain arrays of more than one UIM or MIU motifs, which provide avidity to bind polyUb chains with relatively higher affinity [13,15,16,18-21]. In some UBDs, these arrangements also determine the linkage selective binding for polyUb. For instance, in the tandem UIM of Rap80, each UIM motif binds to a single Ub and the linker between the two motifs determines the orientation of the binding surfaces on the individual UIMs thereby imparting specificity in binding to polyUb of K63 linkage type [18,19].

We recently reported the discovery of a new family of DUBs called MINDY (MIU-containing novel DUB family) that is highly selective at cleaving K48-linked polyUb chains [22]. The first member identified in this family, FAM63A/MINDY-1, contains a tandem MIU repeat (tMIU) that is highly specific for binding to K48-linked polyUb chains. The tMIU enables efficient cleavage of long polyUb chains by MINDY-1. In order to understand the molecular mechanism of how the tMIU of MINDY-1 specifically recognizes K48 chains, we biochemically and biophysically analyzed its Ub binding in detail. Our results reveal an atypical mode of polyUb recognition where the second MIU (MIU2) on its own contains all the specificity determinants. MIU2 makes contacts with all three Ub moieties in a K48-linked polyUb chain via three different binding-sites on the MIU. The first MIU (MIU1) further contributes to polyUb binding through avidity despite itself being a poor binder for polyUb chains. Collectively, our results provide new concepts for polyUb recognition by MIU motifs.

Results and Discussion

MINDY-1 contains a tandem MIU repeat, highly selective at binding K48-polyUb chains

Preferences of tandem UIMs for binding to one linkage type of polyUb chains over the other has been described [13,18,19,23]. However, such analyses were limited to only few chain types, mostly K48 and K63 linkages. Only recently, methods to assemble large quantities of pure polyUb chains of M1, K6, K11, K29, K33, K48 and K63 were established [24-31]. This has been an invaluable tool for UBD linkage profiling that led for instance to the identification of NZF1 of TRABID as a K29- and K33-polyUb selective binder [27]. When profiled against tetraUb of seven linkage types, we confirmed the exclusive preference of Rap80 and Epsin-15 tUIMs for binding to K63 polyUb chains [18,19] (**Fig EV1A**). We found that S5a tUIM that was previously reported to bind K11, K48 and K63 chains also captures M1 polyUb chains [23,32] (**Fig EV1A**). The tandem A20_ZnF-MIU domain of Rabex-5 previously reported to capture M1-, K48- and K63-polyUb chains [15,16,33,34] also binds to tetraUb linked via K6, K11, K29 and K33 (**Fig EV1A**). Our results demonstrate that using a panel of tetraUb chains in Halo-tagged UBD pull-down assays can reveal the linkage preference of a given UBD.

Based on sequence analysis we discovered that two previously uncharacterized proteins, FAM63A and FAM63B, contain a tandem MIU at the C terminus (**Fig 1A-B** and **Fig EV1B-C**). In our recent study, we characterized these two proteins to be DUBs of a novel family, which we named MINDY (MIU-containing novel DUB family) [22]. While the sequences of the MIU motifs are highly conserved between the two proteins, the linker region connecting the two motifs is not (**Fig 1A**). Despite this similarity, the tMIU of FAM63A/MINDY-1 is highly specific for binding to K48 chains whereas the tMIU of FAM63B/MINDY-2 is non-specific and binds to polyUb chains of different linkage types (**Fig 1C**). We therefore wanted to understand how the tMIU of MINDY-1 achieves linkage specificity for K48 chains.

Single MIU motif is sufficient for selective binding to K48 chains

We first evaluated the contribution of each MIU motif of MINDY-1 towards polyUb binding. Mutating the key central alanine of the MIU motif to glycine has been reported to disrupt the motif from binding to monoUb [16]. We therefore mutated the central alanine or deleted the whole motif of MIU1 or MIU2 and tested the effect of such mutations on K48-linked tetraUb

binding. Mutating or deleting MIU1 did not disrupt binding to K48-tetraUb (**Fig 2A** lane 4&6). In contrast, mutating or deleting MIU2 completely abolished binding to K48-tetraUb (**Fig 2A** lane 3&5). These observations were further confirmed in pull-down assays of ubiquitylated materials from HEK293 cells (**Fig 2B**). Together, our data suggest that MIU2 is the dominant polyUb chain binder in MINDY-1.

Tandem UIMs and MIUs have been reported to prefer binding to longer polyUb chains [13,16,20,21,35-38]. Pull downs from HEK293 cell extracts using MINDY-1 tMIU did not capture lower molecular weight polyUb chains, suggesting a preference for binding to longer polyUb chains (**Fig 2B**). To investigate this further, we incubated Halo-tagged tMIU with K48-linked polyUb chains of different lengths that varied from monoUb to pentaUb (**Fig 2C**). We found that the tMIU binds to tri-, tetra- and pentaUb, but does not bind to monoUb and diUb, supporting a preference of tMIU to bind longer polyUb chains. To measure the affinity of the tMIU for polyUb chains of the varying lengths, we performed ITC measurements where MINDY-1 tMIU was titrated into either K48-diUb, triUb or tetraUb (**Fig 2D-F**). We observed affinities of 23 μM, 1.2 μM and 185 nM for diUb, triUb and tetraUb, respectively, suggesting that the affinity of MINDY-1 tMIU for polyUb chains increases with chain length. Collectively, our results demonstrate that MINDY-1 tMIU preferably binds to longer K48-linked polyUb chains.

To explore the role of MIU1 in the binding of MINDY-1 tMIU to polyUb chains, we compared the binding of MIU1 and MIU2 on their own to K48-triUb by ITC. If MIU1 has no role in overall binding, we predict the affinity of MIU2 for K48-triUb to be the same as that observed with tMIU. Consistent with our previous finding, MIU1 on its own has no measurable affinity towards polyUb chains (**Fig 2G**). Surprisingly, we found that the affinity of the tMIU containing both MIU1 and MIU2 for K48-triUb is ten-fold higher than that of MIU2 on its own (**Fig 2H**). This suggests that even though the affinity of the isolated MIU1 for K48-triUb is negligible, it contributes to tMIU binding through avidity.

Since MIU1 only provides weak binding to polyUb chains, we hypothesize that MIU2 is the main determinant of K48-linkage selectivity. When Halo-tagged MIU2 was incubated with a panel of seven types of polyUb chains it only captured K48-tetraUb (**Fig 2I**). This implies that on its own MIU2 is still selective towards K48 linkages and therefore is the linkage specificity determinant in MINDY-1 tMIU.

Cooperativity between MIU1 and MIU2 results in highly selective polyUb interaction

Even though MIU2 is sufficient to capture K48-linked polyUb chains, MIU1 is still required for the tMIU to bind polyUb chains with higher affinity. However, it remains unclear whether MIU1 also contributes to the overall linkage selectivity of the tMIU. To address this, we first explored the contribution of the linker separating the two motifs. One major difference between the K48-linkage-specific MINDY-1 tMIU and the linkage-unspecific MINDY-2 tMIU is their linker length and composition (**Fig 1A**). In Rap80, the linker length in-between two UIM motifs defines the specificity for K63-linked polyUb [18,19]. Therefore, to test whether the linker length and composition of MINDY-1 tMIU regulate polyUb binding, we replaced the 5-residue linker of MINDY-1 tMIU with the one of MINDY-2 tMIU. Swapping the linker made no difference to linkage specificity of the tMIU (**Fig 3A** lane 6). The presence of two proline residues results in a rigid linker (**Fig 1A**). To make the linker relatively flexible, we mutated the two proline residues to alanine or replaced the whole linker with poly-Ser-Gly or poly-Ala linker (**Fig 3A** lane 7-9). Again, we found that altering the composition of the linker does not convert the K48-linkage specificity of the tMIU. In summary, the length and composition of the linker does not affect the specificity of MINDY-1 tMIU for K48-linked polyUb chains.

Despite being very similar to the tMIU of MINDY-1, it is intriguing that the tMIU of MINDY-2 binds to polyUb chains of all linkage types (**Fig 1C**). We therefore characterized the binding properties of the individual MIU motifs of MINDY-2 and found that the first MIU (MIU1) motif of MINDY-2 is the dominant Ub-binder whereas the second motif (MIU2) shows no detectable binding (**Fig 3B**). Further, MINDY-2 MIU1 has no linkage selectivity as it captures polyUb chains of all linkage types (**Fig 3C**). The affinity of MINDY-2 MIU1 on its own to polyUb chains is weaker compared to the tMIU (**Fig 3C** and **1C**). This suggests that similar to MINDY-1, the weak polyUb-binder MIU2 in MINDY-2 also contributes to overall polyUb binding of the tMIU through avidity.

We then wondered whether replacing MIU1 of MINDY-1 with a motif that binds non-selectively to polyUb chains could alter the linkage preference of MINDY-1 tMIU. First we tested if introducing a K48-selective MIU at the position of MIU1, alters the specificity of the tandem MIU. When analyzed, a tandem repeat of the K48-selective MINDY-1 MIU2 is still K48-linkage selective and in fact appears to bind to K48 chains with higher affinity (**Fig 3D** top). Next, we performed a domain swap, where we replaced MINDY-1 MIU1 with the non-

selective polyUb binder of MINDY-2 MIU1. The hybrid tMIU is no longer K48-selective and binds to K6, K11, K48 and K63 chains, which is similar to the profile of MINDY-2 tMIU (**Fig 3D** bottom and **Fig 1C**). Thus, within the tMIU, having a non-selective polyUb binder at the position of MIU1 converts the K48-specific binder to a non-specific one. In summary, the weak polyUb-binding property of MIU1 allows MIU1 to work in synergy with MIU2 to increase the affinity of MINDY-1 tMIU for polyUb without altering its selectivity towards K48-linked polyUb chains.

MIU2 binds to open conformations of K48-linked polyUb chains

To understand how MINDY-1 MIU2 specifically recognizes K48-linked polyUb and how this interaction is enhanced by MIU1, we attempted to crystallize the tMIU in complex with K48-triUb. Unfortunately, we were unable to obtain any crystals. We therefore crystallized the tMIU in complex with K48-diUb and these crystals diffracted to 2.0 Å. The structure was solved by molecular replacement using Ub as a search model. There are two Ub moieties present in the asymmetric unit (ASU) (**Fig 4A**). Although discernible electron density is not present for the linkage between the two Ub moieties, L73 of the distal Ub is pointing towards K48 of the proximal Ub. Clear electron density was visible for a helix, which was manually built in and the structure was refined to the final statistics shown in **Appendix Table S1**. To our surprise, only one 4-turn-helix corresponding to MIU2 (residues 408 to 426) could be modeled into the electron density. The weak affinity of MIU1 for polyUb chains (**Fig 2G**) and the unstructured linker connecting the two MIU motifs might explain the absence of electron density for MIU1.

Interestingly, when we analyzed the crystal packing we found that the diUb from the ASU makes contact with the diUb from the symmetry-related molecule, forming a cyclic K48-linked tetraUb chain (**Fig 4B**). This cyclic chain adopts a doughnut-like shape with two grooves at its center where the two MIU2 molecules bind (**Fig EV2A**). All the I44 patches are no longer at the interface between Ub moieties and therefore, this cyclic K48-tetraUb chain is in an open conformation.

To date, four structures of K48-tetraUb chains have been solved [8,39-41]. In three of these structures (1F9J, 2O6V and 3ALB), K48-linked tetraUb forms cyclic chains. However, these are all in closed conformations where the I44 patches of the all Ub moieties are buried in the interface (**Fig 4C** middle). Even though the other crystal structure of K48-tetraUb is in an

open conformation (1TBE), the fourth and the first Ub moieties are not linked and therefore, is a non-cyclic chain and different from the K48-tetraUb chain observed in this study (**Fig 4C** right). Interestingly, looking further into the symmetry-related molecules, we can also model an open non-cyclic K48-tetraUb (**Fig EV2B**). However, the distance between K48 and G76 of the second and third Ub moieties (~11 Å) is too far-apart for an isopeptide bond to form. Therefore, this conformation is less likely to exist in nature. In summary, we here report a novel structure of open cyclic K48-linked tetraUb chains when in complex with two MINDY-1 MIU2 motifs.

Mechanism of K48-linked triUb recognition by MIU2

The four Ub moieties of the cyclic K48-tetraUb chain are wrapped around the two MIU2 helices (**Fig 4B**). In such an arrangement, a single MIU2 interacts simultaneously with three Ub moieties using three different binding-sites on the MIU2 helix (**Fig 5A-B** and **Fig EV3A**). Only K48-linked polyUb chains can adopt this conformation, as K48 is the only lysine residue within close proximity to the C terminus of the distal Ub (**Fig EV3B**). This structure of MIU2 with K48-linked triUb explains the preference of MINDY-1 to bind to longer polyUb chains (**Fig 2**).

The first binding interface (Site 1) is formed through hydrophobic interactions and hydrogen bonds between MIU2 and the middle Ub (**Fig 5C** and **Fig EV3C**). This mode of binding is similar to the one reported for Rabex-5 MIU and monoUb [15,16]. The conserved A416 of MIU2 is buried deep within the I44 patch of the middle Ub. As with other MIUs and UIMs, mutation of A416 completely abolishes polyUb binding (**Fig 5F** and **Fig EV4C**). L413, L415 and L419 that surround A416 also contribute in binding to I44 patch. The hydrogen bonds are formed between the side chains of D412 and Q420 and the main chains of Ub A46, G47 and L71. In addition to this, the side chains of MIU2 Q420 and Ub R42 and R72 also interact. Indeed, mutating residues D412, Q420 or E423 on MIU2 significantly reduces the tMIU binding to K48-tetraUb, highlighting the importance of these Site 1 interactions (**Fig 5G**). Collectively, these networks of hydrophobic interactions and hydrogen bonds suggest a tight binding of the middle Ub to MIU2.

The second binding interface (Site 2) is formed between MIU2 and the proximal Ub, which occupies a smaller buried surface area of ~240 $Å^2$ in comparison to Site 1 (~500 $Å^2$) and Site 3 (~480 $Å^2$) (**Fig 5A**). The proximal Ub is bound by MIU2 in an unusual way, where a bulky

hydrophobic residue on Site 2, Y424, mediates key interactions – the hydrophobic aromatic ring of Y424 interacts with the I44 patch of the proximal Ub, and the hydroxyl group of Y424 interacts with the main chain amide group of A46 and G47 (**Fig 5D**). These interactions are analogous to MIU2 A416 and D412 on Site 1, respectively (**Fig 5C**). Mutating Y424 to Ala or acidic residues, but not Phe or Trp, abolishes tMIU binding to K48-tetraUb, confirming the crucial role of the hydrophobic aromatic ring for Ub binding (**Fig 5H**). Y424 also interacts with L73 of the middle Ub and therefore highlights the key role of Y424 in stabilizing MIU2 interaction with polyUb. In other MIU motifs, the position corresponding to Y424 is commonly occupied by acidic residues and therefore, the mode of binding by Y424 is a unique feature of MINDY-1 MIU2 (**Fig 5B**).

The third binding interface (Site 3) is formed between MIU2 and the distal Ub, which was determined from crystal contacts with the symmetry-related molecule (**Fig 4A-B**). MIU2 L408, T411, L415 and L419 interact with the hydrophobic patch on the distal Ub formed by I36, P37, L71 and L73 (**Fig 5E**). In addition, the side chains of MIU2 T411, Q418 and Q421 form hydrogen bonds with the main chains of Ub I36, L71 and L8, respectively. Further interactions between the side chains of MIU2 E422 and Ub R72 reinforce the binding. To determine the contribution of Site 3 to polyUb binding, we individually mutated residues forming Site 3. With the exception of L415 and L419, mutation of L408, T411, Q418, Q421 or E422 did not disrupt polyUb binding of the tMIU (**Fig 5F-G** and **Fig 5B**). L415 and L419 also bind to the middle Ub (Site 1) and therefore, the loss of binding observed upon mutating these residues could be a result of simultaneously disrupting Site 1 interaction with the middle Ub.

We postulate that additional interactions mediated by MIU1 with the distal Ub may compensate for the mutations on Site 3 (**Fig 5J**). To test this hypothesis, we mutated residues on Site 3 in MIU2 and found that in the absence of MIU1, mutating L415, Q418 and L419 abolishes binding to polyUb (**Fig 5I**). This suggests that the residual binding of L415, Q418 and L419 mutants observed in tMIU was due to MIU1 binding to Ub. In addition to highlighting the contribution of Site 3 of MIU2 to Ub binding, these observations suggest that MIU2 binding to the distal Ub is enhanced by MIU1 through mechanisms yet to be elucidated (**Fig 5J**).

MIU2 A416 and Y424 bind the middle Ub and proximal Ub, respectively, in an orientation that can only be accommodated by K48-linked diUb, which explains the linkage selectivity

of MIU2 (**Fig EV4A** and **Fig EV3B**). This mode of binding is analogous to Rap80 tUIM, where the linker connecting the two UIMs of Rap80 stretches and positions the interacting surfaces of the two UIMs in an orientation that only K63-linked diUb can accommodate (**Fig EV4B**) [18,19]. Altering the distance between the key alanine residues of the two UIMs abrogates Rap80 tUIM binding to K63 chains [19]. To test if MINDY-1 MIU2 also employs the same mode of binding, we altered the distance between the two binding sites within MIU2 by deleting E423 or introducing Ala residues in-between A416 and Y424 (**Fig EV4D**). Indeed, altering the distance between these two key residues completely disrupts tMIU binding to polyUb chains (**Fig EV4D-F**). These results highlight the importance of the spatial arrangements between two Ub-binding sites within MINDY-1 MIU2 to bind and orient Ub moieties within K48-linked polyUb chains.

Individual UIM motifs in Hrs and AIRAPL have been reported to contain multiple Ub-binding sites [20,42]. Hrs UIM has two hydrophobic strips on either side of its helix, which each binds to the I44 patch of independent Ub molecule [42]. The two Ub molecules bound to Hrs are not linked by any isopeptide bond and therefore, the double-sided Ub-binding on Hrs UIM does not provide linkage specificity but a higher efficiency in binding to multiple monoubiquitylated cargoes in the endocytic pathway [42]. On the other hand, the tUIM of AIRAPL recognizes K48-linked triUb where the two Ub-binding sites on UIM2 bind to two moieties of Ub simultaneously, whereas UIM1 binds to the proximal Ub [20]. Even though AIRAPL UIM2 was described as the K48 linkage determinant for the tUIM, in the absence of UIM1, UIM2 failed to bind K48-triUb. In contrast, MINDY-1 MIU2 uses distinct mechanisms in which the three Ub-binding sites simultaneously bind to all three Ub moieties (**Fig 5J**).

K48-linked polyUb chains are flexible and adopt different conformations as both open and closed chains have been reported for unbound chains [9]. However, all structures of K48-linked diUb chains in complex with their binding partners are found in open conformations where at least one of the two I44 patches is occupied [20,43-47]. The two K48-diUb chains bound to MINDY-1 MIU2 are also in open conformations and suggest a preference for UBDs to bind to K48 chains in more extended conformations (**Figure EV2C**). In contrast, K63-linked polyUb chains in complex with their binding partners have been observed in both open and closed chain conformations [48]. It is intriguing that none of the UBDs analyzed to date recognize and bind to the closed conformation of K48 chains.

It is interesting that MINDY-1 tMIU, in addition to sensing polyUb chain linkage type can also select for chain length (**Fig 2**). In our recent study we demonstrated that tMIU is required for MINDY-1 DUB activity in hydrolyzing long K48-linked polyUb chains [22]. In the present study we observe that MINDY-1 MIU2 binds to K48-polyUb chains in open conformations (**Fig 5A**). We hypothesize that the tMIU helps MINDY-1 to bind to the regions where long K48 chains are in open conformations, and therefore facilitates the DUB to bind to its substrate (**Fig EV4G**).

Our study also reveals that despite its sequence similarity with MINDY-1 tMIU, FAM63B/MINDY-2 tMIU is completely non-specific for any particular linkage type (**Fig 1C**). Interestingly, full length MINDY-2 selectively hydrolyzes only K48 chains [22]. These observations suggest that the tMIU of MINDY-2 may enable the enzyme to process mixed and branched Ub types. Future work will elucidate how the UBD and the catalytic domain of MINDY-1 and MINDY-2 work together in a cellular context.

Materials and Methods

cDNA clones and antibodies

All cDNA clones were generated by the DNA cloning team, Medical Research Council Protein Phosphorylation and Ubiquitylation Unit (MRC PPU) Reagents and Services, University of Dundee, United Kingdom (**Appendix Table S2**). Anti-Ub was purchased from DAKO (Z0458).

Halo-UBD expression and purification

UBDs were cloned as fusion proteins with an N-terminal GST tag or a tandem GST-Halo tag (**Appendix Table S2**). Recombinant proteins were expressed in *E. coli* strain BL21 grown in 2xTY media containing 100 µg/ml ampicillin. Cells were induced with 300 µM isopropyl b-D-1-thiogalactopyranoside (IPTG) at an OD_{600} of 0.6-0.8 and grown for 16 h at 16 °C. Cells were pelleted and resuspended in 50 mM Tris pH 7.5, 300 mM NaCl, 10% glycerol, 0.075% 2-mercaptoethanol, 1 mM benzamidine, 1 mM AEBSF and protease inhibitor cocktail (Roche). Cell lysis was carried out by sonication. After being clarified through centrifugation, bacterial lysate was incubated with Glutathione Sepharose 4B resin (GE Healthcare) for 2 h at 4 °C. The resin bound proteins were washed extensively with high salt buffer (25 mM Tris pH 7.5, 500 mM NaCl, and 1 mM DTT) and low salt buffer (25 mM Tris pH 7.5, 150 mM NaCl, 10% glycerol, and 1 mM DTT). Halo-tag UBD was eluted by cleaving off the GST tag

using C3 protease. The purified proteins were concentrated, flash frozen in liquid nitrogen and stored at -80 °C.

Assembly and purification of polyubiquitin chains of defined lengths

PolyUb chains were assembled enzymatically in reactions containing 1500 µM Ub (Sigma Aldrich), 50 mM Tris pH 7.5, 10 mM $MgCl_2$, 0.6 mM DTT and 10 mM ATP, incubated at 30 °C for the indicated period of time. M1 chains were assembled for 2 h in the presence of 1 µM UBE1, 10 µM UBE2L3 and 10 µM HOIP [24]. K6 chains were assembled for 3 h in the presence of 0.5 µM UBE1, 9.5 µM UBE2L3, 12.40 µM NleL (170-782) and 5 µM OTUB1 [25]. K11 chains were assembled for 6 h in the presence of 1 µM UBE1, 40 µM UBE2S-UBP and 2 µM AMSH [26]. Fresh DUB was added and the reaction was incubated for another 16 h. K29 chains were assembled for 6 h in the presence of 0.64 µM UBE1, 9.5 µM UBE2D3 and 3 µM UBE3C [27]. K33 chains were assembled for 6 h in the presence of 0.5 µM UBE1, 9 µM UBE2D1 and 6.3 µM AREL1 [28]. In the K29 and K33 chains assembly, DUBs (2 µM vOTU for K29, and 5 µM OTUB1 + 20 µM Cezanne E287K/E288K for K33) were added after the 6 h incubation and the reaction was incubated for another 16 h. K48 chains were assembled for 6 h in the presence of 1 µM UBE1 and 25 µM UBE2R1 [49]. K63 chains were assembled for 3 h in the presence of 1 µM UBE1, 10 µM UBE2N and 20 µM UBE2V1 [49].

At the end of the assembly reaction, enzymes used in the reaction were precipitated by the addition of a total volume of 50 ml of 50 mM sodium acetate pH 4.5. After at least 3 h incubation at 4 °C, the solution was filtered (0.22-µm). DiUb, triUb, tetraUb, and pentaUb were purified by cation exchange using a ResourceS 6 ml column (GE Healthcare), equilibrated in 50 mM sodium acetate pH 4.5, and eluted in a gradient with elution buffer (50 mM sodium acetate pH 4.5 and 1 M NaCl). Peak fractions containing di-, tri-, tetra- and pentaUb chains were concentrated and buffer exchanged to 20 mM Tris pH 7.5.

UBD linkage selectivity profiling assays

Halo-tagged UBDs (10.5 nmol) was incubated with 100 µl of the HaloLink resin (Promega) in 500 µl of the coupling buffer (50 mM Tris pH 7.5, 150 mM NaCl, 0.05% NP-40 substitute and 1 mM DTT) for 2 h at 4 °C. The UBD linkage selectivity analysis was carried out by incubating 10 µl of the coupled Halo-UBD with 29 pmol of tetraUb of the indicated linkages in 500 µl of pull down buffer (50 mM Tris pH 7.5, 150 mM NaCl, 0.1% NP-40, 1 mM DTT, 0.5 mg/ml BSA) for 2 h at 4 °C. The resin was washed two times with the wash buffer (50 mM Tris pH 7.5, 250 mM NaCl, 0.2% NP-40, 1 mM DTT) and once with the coupling

buffer. Captured tetraUb chains were eluted by adding LDS buffer, separated on 4-12% SDS-PAGE gel (Life Technology), and visualized by silver staining using Pierce Silver stain kit (ThermoFischer).

Isothermal titration calorimetry (ITC)

ITC measurements were performed on a MicroCal PEAQ-ITC (Malvern) at 25 °C with a setting of 20 × 2 µl injections. All proteins were dialyzed into 50 mM Hepes pH 7.5, 150 mM NaCl and 250 µM TCEP. For all measurements, the syringe contained UBD at a concentration of 300 µM, and the cell contained polyUb chains at a concentration of 30 µM.

Crystallization and structure determination of MINDY-1 tMIU:K48-diUb

Purified MINDY-1 tMIU (untagged) and K48-linked diUb were mixed in 1:1 ratio at 400 nmol each. After an 16 h incubation, the protein complex was concentrated to 16.3 mg/ml. Crystals were grown using vapor diffusion technique in mother liquor containing 100 mM sodium acetate pH 5.4 and 18.5 % PEG3350. Crystals were cryo-protected in mother liquor containing 30% PEG400 before vitrification in liquid nitrogen. Diffraction data was collected at ID30A of the European Synchrotron Radiation Facility (Grenoble, France). Data was processed and scaled using XDS [50] and merged using AIMLESS [51]. The structure was solved by molecular replacement using Ub (1UBQ [52]) as a search model in Phaser [53]. Iterative rounds of refinements were done using REFMAC5 [54] with model building in COOT [55]. The structure was finally re-refined using PDB_REDO [56]. The final data collection and refinement statistics are shown in Table 1.

The structure was analyzed with PIC and PISA [57,58]. Figures were made with the PyMOL Molecular Graphics System, Schrödinger, LLC (https://www.pymol.org/).

Accession code

Coordinates for MINDY-1 tMIU:K48-diUb complex have been deposited at the Protein Data Bank under accession codes 5MN9.

Acknowledgements

We thank V.K. Chaugule and S. Lange for discussions and critical comments on the manuscript. This work was supported by the Medical Research Council UK (MC_UU_12016/6 - Ubiquitin signalling mechanisms), Tenovus Scotland, EMBO Young Investigator Programme and the pharmaceutical companies supporting the Division of Signal

Transduction Therapy (AstraZeneca, Boehringer-Ingelheim, GlaxoSmithKline, Merck KGaA, Janssen Pharmaceutica, and Pfizer).

Author contributions

Y.A.K. performed all experiments. Y.A.K. and Y.K. designed experiments and analyzed data. S.A.A.R. performed crystallographic analyses. S.W. cloned all the DNA constructs. A.K. provided enzymes used in the polyUb assembly and K48-polyUb chains used in the ITC experiments. Y.A.K. and Y.K. wrote the manuscript with input from all authors.

Conflict of interest

The authors declare that they have no conflict of interest.

References

1. Chen ZJ (2005) Ubiquitin signalling in the NF-κB pathway. *Nat Cell Biol* **7**: 758–765.
2. Ulrich HD, Walden H (2010) Ubiquitin signalling in DNA replication and repair. *Nat Rev Mol Cell Biol* **11**: 479–489.
3. MacGurn JA, Hsu P-C, Emr SD (2012) Ubiquitin and membrane protein turnover: from cradle to grave. *Annu Rev Biochem* **81**: 231–259.
4. Bhattacharyya S, Yu H, Mim C, Matouschek A (2014) Regulated protein turnover: snapshots of the proteasome in action. *Nat Rev Mol Cell Biol* **15**: 122–133.
5. Pickart CM, Eddins MJ (2004) Ubiquitin: structures, functions, mechanisms. *Biochim Biophys Acta* **1695**: 55–72.
6. Kulathu Y, Komander D (2012) Atypical ubiquitylation - the unexplored world of polyubiquitin beyond Lys48 and Lys63 linkages. *Nat Rev Mol Cell Biol* **13**: 508–523.
7. Cook WJ, Jeffrey LC, Carson M, Chen Z, Pickart CM (1992) Structure of a diubiquitin conjugate and a model for interaction with ubiquitin conjugating enzyme (E2). *J Biol Chem* **267**: 16467–16471.
8. Cook WJ, Jeffrey LC, Kasperek E, Pickart CM (1994) Structure of tetraubiquitin shows how multiubiquitin chains can be formed. *J Mol Biol* **236**: 601–609.
9. Varadan R, Walker O, Pickart C, Fushman D (2002) Structural properties of polyubiquitin chains in solution. *J Mol Biol* **324**: 637–647.
10. Husnjak K, Dikic I (2012) Ubiquitin-binding proteins: decoders of ubiquitin-mediated cellular functions. *Annu Rev Biochem* **81**: 291–322.
11. Clague MJ, Barsukov I, Coulson JM, Liu H, Rigden DJ, Urbé S (2013) Deubiquitylases from genes to organism. *Physiol Rev* **93**: 1289–1315.
12. He F, Wollscheid H-P, Nowicka U, Biancospino M, Valentini E, Ehlinger A, Acconcia F, Magistrati E, Polo S, Walters KJ (2016) Myosin VI contains a compact structural motif that binds to ubiquitin chains. *Cell Rep* **14**: 2683–2694.
13. Young P, Deveraux Q, Beal RE, Pickart CM, Rechsteiner M (1998) Characterization of two polyubiquitin binding sites in the 26 S protease subunit 5a. *J Biol Chem* **273**: 5461–5467.
14. Hofmann K, Falquet L (2001) A ubiquitin-interacting motif conserved in components of the proteasomal and lysosomal protein degradation systems. *Trends Biochem Sci* **26**: 347–350.
15. Lee S, Tsai YC, Mattera R, Smith WJ, Kostelansky MS, Weissman AM, Bonifacino JS, Hurley JH (2006) Structural basis for ubiquitin recognition and autoubiquitination by Rabex-5. *Nat Struct Mol Biol* **13**: 264–271.
16. Penengo L, Mapelli M, Murachelli AG, Confalonieri S, Magri L, Musacchio A, Di Fiore PP, Polo S, Schneider TR (2006) Crystal structure of the ubiquitin binding domains of Rabex-5 reveals two modes of interaction with ubiquitin. *Cell* **124**: 1183–1195.
17. Hurley JH, Lee S, Prag G (2006) Ubiquitin-binding domains. *Biochem J* **399**: 361–372.
18. Sims JJ, Cohen RE (2009) Linkage-specific avidity defines the lysine 63-linked polyubiquitin-binding preference of Rap80. *Mol Cell* **33**: 775–783.
19. Sato Y, Yoshikawa A, Mimura H, Yamashita M, Yamagata A, Fukai S (2009) Structural basis for specific recognition of Lys 63-linked polyubiquitin chains by tandem UIMs of RAP80. *EMBO J* **28**: 2461–2468.
20. Rahighi S, Braunstein I, Ternette N, Kessler B, Kawasaki M, Kato R, Matsui T, Weiss TM, Stanhill A, Wakatsuki S (2016) Selective binding of AIRAPL tandem UIMs to Lys48-linked tri-ubiquitin chains. *Structure* **24**: 412–422.
21. Burnett B, Li F, Pittman RN (2003) The polyglutamine neurodegenerative protein ataxin-3 binds polyubiquitylated proteins and has ubiquitin protease activity. *Hum Mol Genet* **12**: 3195–3205.
22. Abdul Rehman SA, Kristariyanto YA, Choi SY, Nkosi PJ, Weidlich S, Labib K, Hofmann K, Kulathu Y (2016) MINDY-1 is a member of an evolutionarily conserved and structurally distinct new family of deubiquitinating enzymes. *Mol Cell* **63**: 146–155.
23. Wang Q, Young P, Walters KJ (2005) Structure of S5a bound to monoubiquitin provides a model for polyubiquitin recognition. *J Mol Biol* **348**: 727–739.
24. Stieglitz B, Morris Davies AC, Koliopoulos MG, Christodoulou E, Rittinger K (2012)

LUBAC synthesizes linear ubiquitin chains via a thioester intermediate. *EMBO Rep* **13**: 840–846.
25. Hospenthal MK, Freund SMV, Komander D (2013) Assembly, analysis and architecture of atypical ubiquitin chains. *Nat Struct Mol Biol* **20**: 555–565.
26. Bremm A, Freund SMV, Komander D (2010) Lys11-linked ubiquitin chains adopt compact conformations and are preferentially hydrolyzed by the deubiquitinase Cezanne. *Nat Struct Mol Biol* **17**: 939–947.
27. Kristariyanto YA, Abdul Rehman SA, Campbell DG, Morrice NA, Johnson C, Toth R, Kulathu Y (2015) K29-selective ubiquitin binding domain reveals structural basis of specificity and heterotypic nature of K29 polyubiquitin. *Mol Cell* **58**: 83–94.
28. Kristariyanto YA, Choi SY, Rehman SAA, Ritorto MS, Campbell DG, Morrice NA, Toth R, Kulathu Y (2015) Assembly and structure of Lys33-linked polyubiquitin reveals distinct conformations. *Biochem J* **467**: 345–352.
29. Michel MA, Elliott PR, Swatek KN, Simicek M, Pruneda JN, Wagstaff JL, Freund SMV, Komander D (2015) Assembly and specific recognition of K29- and K33-linked polyubiquitin. *Mol Cell* **58**: 95–109.
30. Raasi S, Pickart CM (2005) Ubiquitin chain synthesis. *Methods Mol Biol* **301**: 47–55.
31. Dong KC, Helgason E, Yu C, Phu L, Arnott DP, Bosanac I, Compaan DM, Huang OW, Fedorova AV, Kirkpatrick DS, et al. (2011) Preparation of distinct ubiquitin chain reagents of high purity and yield. *Structure* **19**: 1053–1063.
32. Baboshina OV, Haas AL (1996) Novel multiubiquitin chain linkages catalyzed by the conjugating enzymes E2EPF and RAD6 are recognized by 26 S proteasome subunit 5. *J Biol Chem* **271**: 2823–2831.
33. Sokratous K, Roach LV, Channing D, Strachan J, Long J, Searle MS, Layfield R, Oldham NJ (2012) Probing affinity and ubiquitin linkage selectivity of ubiquitin-binding domains using mass spectrometry. *J Am Chem Soc* **134**: 6416–6424.
34. Shin D, Lee SY, Han S, Ren S, Kim S, Aikawa Y, Lee S (2012) Differential polyubiquitin recognition by tandem ubiquitin binding domains of Rabex-5. *Biochem Biophys Res Commun* **423**: 757–762.
35. Swanson KA, Kang RS, Stamenova SD, Hicke L, Radhakrishnan I (2003) Solution structure of Vps27 UIM-ubiquitin complex important for endosomal sorting and receptor downregulation. *EMBO J* **22**: 4597–4606.
36. Raasi S, Orlov I, Fleming KG, Pickart CM (2004) Binding of polyubiquitin chains to ubiquitin-associated (UBA) domains of HHR23A. *J Mol Biol* **341**: 1367–1379.
37. Chai Y, Berke SS, Cohen RE, Paulson HL (2004) Poly-ubiquitin binding by the polyglutamine disease protein ataxin-3 links its normal function to protein surveillance pathways. *J Biol Chem* **279**: 3605–3611.
38. Pinato S, Scandiuzzi C, Arnaudo N, Citterio E, Gaudino G, Penengo L (2009) RNF168, a new RING finger, MIU-containing protein that modifies chromatin by ubiquitination of histones H2A and H2AX. *BMC Mol Biol* **10**: 55.
39. Phillips CL, Thrower J, Pickart CM, Hill CP (2001) Structure of a new crystal form of tetraubiquitin. *Acta Crystallogr D Biol Crystallogr* **57**: 341–344.
40. Eddins MJ, Varadan R, Fushman D, Pickart CM, Wolberger C (2007) Crystal structure and solution NMR studies of Lys48-linked tetraubiquitin at neutral pH. *J Mol Biol* **367**: 204–211.
41. Satoh T, Sakata E, Yamamoto S, Yamaguchi Y, Sumiyoshi A, Wakatsuki S, Kato K (2010) Crystal structure of cyclic Lys48-linked tetraubiquitin. *Biochem Biophys Res Commun* **400**: 329–333.
42. Hirano S, Kawasaki M, Ura H, Kato R, Raiborg C, Stenmark H, Wakatsuki S (2006) Double-sided ubiquitin binding of Hrs-UIM in endosomal protein sorting. *Nat Struct Mol Biol* **13**: 272–277.
43. Varadan R, Assfalg M, Raasi S, Pickart C, Fushman D (2005) Structural determinants for selective recognition of a Lys48-linked polyubiquitin chain by a UBA domain. *Mol Cell* **18**: 687–698.
44. Zhang N, Wang Q, Ehlinger A, Randles L, Lary JW, Kang Y, Haririnia A, Storaska AJ, Cole JL, Fushman D, et al. (2009) Structure of the S5a:K48-Linked diubiquitin complex and its

interactions with Rpn13. *Mol Cell* **35**: 280–290.
45. Liu S, Chen Y, Li J, Huang T, Tarasov S, King A, Weissman AM, Byrd RA, Das R (2012) Promiscuous interactions of gp78 E3 ligase CUE domain with polyubiquitin chains. *Structure* **20**: 2138–2150.
46. Shi Y, Chen X, Elsasser S, Stocks BB, Tian G, Lee B-H, Shi Y, Zhang N, de Poot SAH, Tuebing F, et al. (2016) Rpn1 provides adjacent receptor sites for substrate binding and deubiquitination by the proteasome. *Science* **351**: 831.
47. Békés M, van der Heden van Noort GJ, Ekkebus R, Ovaa H, Huang TT, Lima CD (2016) Recognition of Lys48-linked di-ubiquitin and deubiquitinating activities of the SARS Coronavirus Papain-like protease. *Mol Cell* **62**: 572–585.
48. Liu Z, Gong Z, Jiang W-X, Yang J, Zhu W-K, Guo D-C, Zhang W-P, Liu M-L, Tang C (2015) Lys63-linked ubiquitin chain adopts multiple conformational states for specific target recognition. *eLife* **4**: e05767.
49. Komander D, Lord CJ, Scheel H, Swift S, Hofmann K, Ashworth A, Barford D (2008) The structure of the CYLD USP domain explains its specificity for Lys63-linked polyubiquitin and reveals a B box module. *Mol Cell* **29**: 451–464.
50. Kabsch W (2010) XDS. *Acta Crystallogr D Biol Crystallogr* **66**: 125–132.
51. Evans PR, Murshudov GN (2013) How good are my data and what is the resolution? *Acta Crystallogr D Biol Crystallogr* **69**: 1204–1214.
52. Vijay-Kumar S, Bugg CE, Cook WJ (1987) Structure of ubiquitin refined at 1.8 Å resolution. *J Mol Biol* **194**: 531–544.
53. McCoy AJ, Grosse-Kunstleve RW, Storoni LC, Read RJ (2005) Likelihood-enhanced fast translation functions. *Acta Crystallogr D Biol Crystallogr* **61**: 458–464.
54. Vagin AA, Steiner RA, Lebedev AA, Potterton L, McNicholas S, Long F, Murshudov GN (2004) REFMAC5 dictionary: organization of prior chemical knowledge and guidelines for its use. *Acta Crystallogr D Biol Crystallogr* **60**: 2184–2195.
55. Emsley P, Lohkamp B, Scott WG, Cowtan K (2010) Features and development of Coot. *Acta Crystallogr D Biol Crystallogr* **66**: 486–501.
56. Joosten RP, Long F, Murshudov GN, Perrakis A (2014) The PDB_REDO server for macromolecular structure model optimization. *IUCrJ* **1**: 213–220.
57. Tina KG, Bhadra R, Srinivasan N (2007) PIC: protein interactions calculator. *Nucleic Acids Res* **35**: W473–W476.
58. Krissinel E, Henrick K (2007) Inference of macromolecular assemblies from crystalline state. *J Mol Biol* **372**: 774–797.
59. Waterhouse AM, Procter JB, Martin DMA, Clamp M, Barton GJ (2009) Jalview Version 2--a multiple sequence alignment editor and analysis workbench. *Bioinformatics* **25**: 1189–1191.

Figure Legends

Figure 1. Linkage selectivity in tandem MIU repeats of MINDY-1

(A) Sequence alignment of MINDY-1/FAM63A and MINDY-2/FAM63B tMIUs from different species. MIU1, MIU2 and the tMIU linker are indicated. The conserved motif of MIU is shown: ϕ, large hydrophobic; #, acidic; x, any residues. *Hs*, *Homo sapiens*; *Pa, Pongo Abelii; Bt*, *Bos taurus; Mm*, *Mus musculus*; Rn, *Rattus norvegicus*. Protein sequences were retrieved from Uniprot database, aligned using the ClustalO program and edited with the Jalview software [59].

(B) Schematic representation of MINDY-1 and MINDY-2 domains. The MIU motifs of MINDY-1 and MINDY-2 are colored red and blue, respectively.

(C) PolyUb linkage selectivity profiling for MINDY-1 and MINDY-2 tMIU. TetraUb chains of the indicated linkage types (29 pmol) were incubated with 1.05 nmol Halo-tagged tUIM of MINDY-1 or MINDY-2 immobilized on HaloLink resin for 2 h at 4 °C. The captured materials were analyzed on silver-stained 4-12% SDS-PAGE gel.

Figure 2. MIU2 is sufficient for binding to K48 chains

(A) K48-linked tetraUb chains were captured by Halo-tagged tMIU wild-type or mutants of MINDY-1 as in Fig 1C. Red and grey squares indicate wild-type and mutant MIU (Ala-to-Gly), respectively.

(B) HEK293 cell lysates (1 mg) were incubated with 1.05 nmol Halo-tagged tMIU wild-type or mutants. The captured Ub was visualized by anti-Ub immunoblotting.

(C) MonoUb and K48-linked polyUb chains of different lengths (29 pmol each) were incubated with 1.05 nmol of Halo-tagged tMIU. The captured materials were visualized as in Fig 1C. Asterisks indicate non-specific bands from Halo-UBD, which exhibit a similar electrophoretic mobility as tri- and pentaUb.

(D-F) ITC measurements for MINDY-1 tMIU binding to K48-linked diUb (D), triUb (E), and tetraUb (F). K_d value of each measurement is indicated.

(G-H) ITC measurements for MINDY-1 MIU1 (G) and MIU2 (H) binding to K48-linked triUb. K_d value of each measurement is indicated.

(I) PolyUb linkage selectivity assay of MINDY-1 MIU2 was carried out as in Fig 1C. Asterisk indicates non-specific bands from Halo-UBD.

Figure 3. Synergy between MIU1 and MIU2 in polyUb binding

(A) M1-, K48- and K63-tetraUb chains were mixed in equal amount of 29 pmol each and incubated with 1.05 nM Halo-MINDY-1 tMIU with wild-type or mutant linkers. The captured materials were analyzed as in Fig 1C. Asterisks indicate non-specific bands from Halo-UBD, which run at the similar electrophoretic mobility as K63-tetraUb.
(B) K48- or K63-linked tetraUb chains were captured by Halo-tagged tMIU wild-type or mutants of MINDY-2 as in Fig 2A. Blue and grey squares indicate wild-type and mutant MIU (Ala-to-Gly), respectively. Asterisks indicate non-specific bands from Halo-UBD.
(C) PolyUb linkage selectivity assay of MINDY-2 MIU1 was carried out as in Fig 1C. Asterisks indicate non-specific bands from Halo-UBD.
(D) PolyUb linkage selectivity assays of hybrid tMIUs were carried out as in Fig 1C. The first MIU motif of MINDY-1 tMIU was replaced by MINDY-1 MIU2 (top) or MINDY-2 MIU1 (bottom). Asterisks indicate non-specific bands from Halo-UBD, which have a similar electrophoretic mobility as M1- and K63-tetraUb chains.

Figure 4. Crystal structure of K48-diUb in complex with MINDY-1 MIU2

(A) Structure of MINDY-1 MIU2 and K48-diUb complex within an asymmetric unit (ASU) with $2|F_O|-|F_C|$ (blue) electron density maps for MIU2 contoured at 1σ. Proximal (light cyan) and distal (blue) are in cartoon representation and MIU2 (salmon) is in sticks.
(B) Open cyclic K48-linked tetraUb chains. Ub moiety #1 (light cyan), #2 (blue) and MIU2 moiety #1 (salmon) are from the ASU. Ub moiety #3 (teal), #4 (green) and MIU2 moiety #2 (salmon) are from the symmetry-related molecules. K48 and the C-terminal tail of Ub moieties are indicated.
(C) Comparison of different K48-linked tetraUb conformations. Schematic diagram illustrates the coloring and numbering of Ub moieties, which are the same as for Fig 4B. K48 and C-terminal tail are shown in red-sticks and spheres, respectively. For simplicity, only I44 is shown in blue spheres to represent the hydrophobic I44 patch (L8, I44, H68 and V70). PDB ID: 1TBE [8] and 1F9J [39].

Figure 5. Mechanism of polyUb chain recognition by MIU2

(A) Structure of MIU2 in complex with K48-linked triUb is shown in cartoon. K48-triUb proximal (light cyan) and middle (blue) Ub are from asymmetric unit, while the distal Ub (teal) is from symmetry related molecule (**Fig 4B**). K48 and the C-terminal tail of Ub are

indicated.

(B) Sequence alignment of MIU motifs from various proteins. All sequences are from *H. sapiens*, except for YPL191C and YGL082W, which are from *S. cerevisiae*. Residues of MINDY-1 MIU2 that form the three Ub-binding sites are indicated. The conserved motif of MIU is shown: ϕ, large hydrophobic; #, acidic; x, any residues.

(C-E) Close-up views of interactions between MINDY-1 MIU2 and the middle Ub (Site 1), proximal Ub (Site 2), distal Ub (Site 3). Hydrophobic interactions and hydrogen bonds are shown on the top and bottom panels, respectively. Residues at the interface are shown in sticks and colored as in Fig 5A. Dotted lines indicate hydrogen bonds.

(F-G) Residues of MIU2 involved in hydrophobic interactions (F) and hydrogen bonds (G) were mutated and the effect on tMIU binding to K48-tetraUb was investigated as in Fig 2A.

(H) Role of Y424 in tMIU binding to K48-tetraUb was investigated by mutating MIU2 Y424 to the indicated residues and pulldown assays were performed as in Fig 2A.

(I) Residues of MIU2 forming Site 3 binding site were mutated and the effect on MIU2 binding to K48-tetraUb was investigated as in Fig 2A.

(J) A model of how MINDY-1 tMIU achieves its K48-linkage selectivity. Three Ub-binding sites on MIU2 engage the I44 patches of the middle and proximal Ub, and the I36 patch of the distal Ub.

Figure EV1. tMIU and tUIM from various proteins display different linkage preference for polyUb chains

(A) Linkage selectivity profile of tUIMs from Rap80, Epsin-15 and S5a, and tandem RUZ-MIU from Rabex-5. The assays were performed as in Fig 1C.

(B) Sequence alignments of the C-terminal UBD region of FAM63A/MINDY-1 from the indicated species.

(C) Sequence alignments of the C-terminal UBD region FAM63B/MINDY-2 from the indicated species. Sequence boundaries of MINDY-1 and MINDY-2 MIU motifs used in this studies are shown. The conserved motif of MIU is shown: ϕ, large hydrophobic; #, acidic; x, any residues.

Figure EV2. Crystal structure of K48-diUb in complex with MINDY-1 MIU2

(A) The cyclic open K48-linked tetraUb forms a doughnut-like shape with two grooves at center where two MIU2 helices bind. Four Ub moieties in Fig 4B are shown in white surface

representation. The structure is rotated on the y-axis to show three different orientations. I44 patch (L8, I44, H68 and V70) is colored blue.

(B) A non-cyclic open conformation of K48-lined tetraUb can also be modeled from symmetry-related molecules of the structure of K48-diUb in complex with MINDY-1 MIU2. Structures are presented as in Fig 4B. Ub moieties within the asymmetric unit are indicated with dotted boxes. Red dotted line indicates the distance between Ub #2 K48 and Ub #3 G76.

(C) The two K48-diUb chains bound to MIU2 are in open conformations. Unbound K48-diUb (PDB ID: 1AAR [7]) is colored grey and white for distal and proximal Ub, respectively. Two K48-linked diUb chains in cartoon are shown in complex with MIU2 in ribbon and colored as in Fig 5A. Il44 is shown as blue spheres. K48 and C-terminal tail are shown in red-sticks and spheres, respectively.

Figure EV3. Structure of MIU2 in complex with K48-triUb

(A) Crystal structure of MIU2 in complex with K48-triUb is shown in two orientations, rotated on the y-axis. Ub moieties are shown in white surface. The two hydrophobic patches of Ub: I44 patch (L8, I44, H68 and V70) and I36 (I36, L71 and L73) are colored blue and green, respectively.

(B) Crystal structure of MIU2:K48-triUb complex is represented in ribbon. Lysine residues of the Ub moieties are shown in sticks and spheres. The distances between C-terminal tail of the middle Ub and the K48 or K6 of the proximal Ub are shown.

(C-E) Surface representations of the three binding sites between MIU2 and K48-linked triUb. Residues involved in hydrophobic interactions and hydrogen bonds are colored red and orange, respectively. Yellow surface indicates portion of the residues at the binding interface that are not directly involved in hydrophobic interactions or hydrogen bonding.

Figure EV4. Role of the distance between Ub-binding sites in MIU2 in driving selectivity

(A-B) K48-diUb (orange) (A) and K63-diUb (green) (B) in complex with MINDY-1 MIU2 and Rap80 tUIM, respectively are shown in cartoon. The distal moieties of the two diUb chains were superposed. The N- and C-terminal ends of MIU2 and tUIM are indicated. The key residues of MIU/UIM that engage with I44 (blue spheres) are shown in sticks. The linker of Rap80 tUIM is colored red. PDB ID: 3A1Q [19].

(C) MIU2 A416 was mutated to Gly, Ser and Asp, and the effect on tMIU binding to K48-tetraUb was investigated as in Fig 2A.

(D-E) The distance between two Ub-binding sites on MIU2 was altered by deleting E423 or inserting Ala residues N terminus to Y424 (D). The effect of mutations on MINDY-1 tMIU binding to K48-tetraUb was investigated as in Fig 2A (E).

(F) As in Fig EV4E, but the effect of the mutations on MINDY-1 tMIU binding to tetraUb of seven linkage types were investigated. Asterisks indicate non-specific bands from Halo-UBD, which has a similar electrophoretic mobility as K63-tetraUb.

(G) A model of how tMIU contributes to the efficiency of long K48-linked polyUb chains hydrolysis by MINDY-1 DUB. The hydrophobic I44 patches are colored in blue and illustrate the open and closed conformations of the polyUb chains.

Figure 1

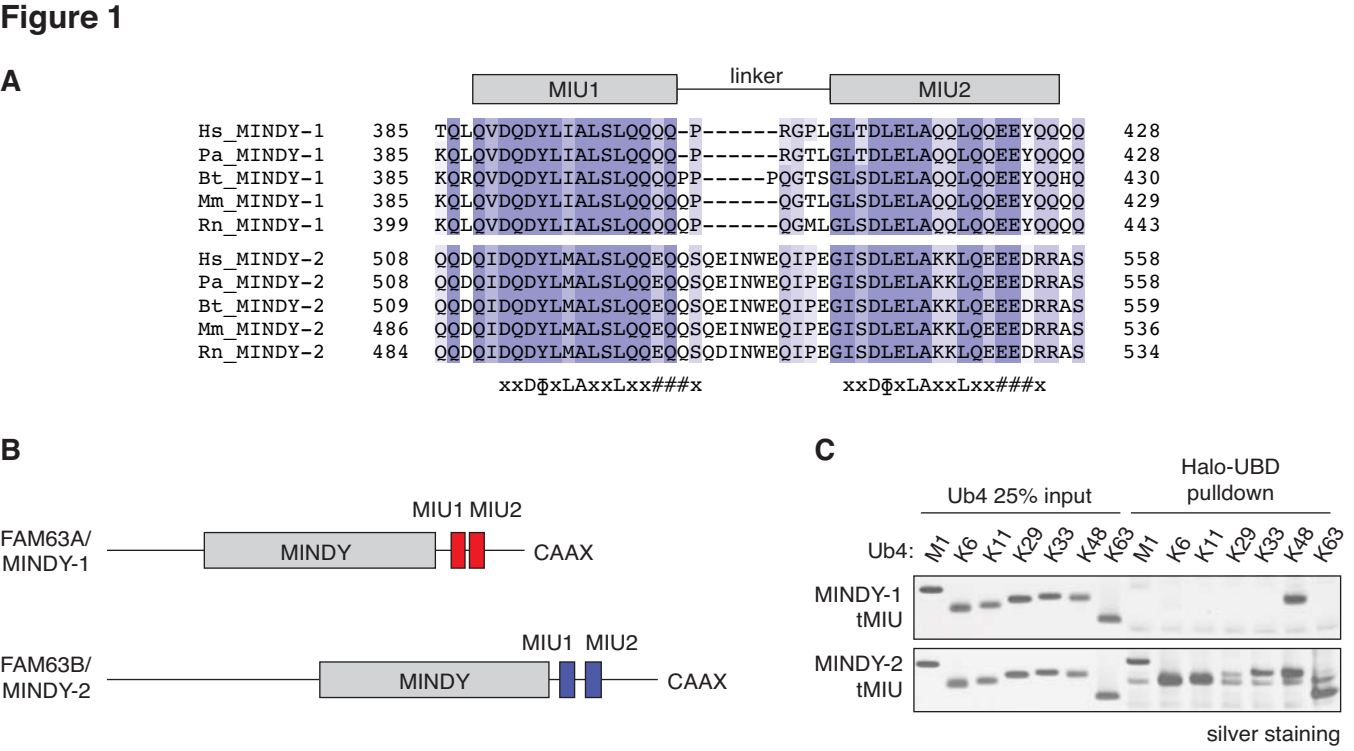
A
MIU1
linker
MIU2
Hs_MINDY-1 385 TQLQVDQDYLIALSLQQQQ-P------RGPLGLTDLELAQQLQQEEYQQQQ 428
Pa_MINDY-1 385 KQLQVDQDYLIALSLQQQQ-P------RGTLGLTDLELAQQLQQEEYQQQQ 428
Bt_MINDY-1 385 KQRQVDQDYLIALSLQQQQPP-----PQGTSGLSDLELAQQLQQEEYQQHQ 430
Mm_MINDY-1 385 KQLQVDQDYLIALSLQQQQQP------QGTLGLSDLELAQQLQQEEYQQQQ 429
Rn_MINDY-1 399 KQLQVDQDYLIALSLQQQQQP------QGMLGLSDLELAQQLQQEEYQQQQ 443
Hs_MINDY-2 508 QQDQIDQDYLMALSLQQEQQSQEINWEQIPEGISDLELAKKLQEEEDRRAS 558
Pa_MINDY-2 508 QQDQIDQDYLMALSLQQEQQSQEINWEQIPEGISDLELAKKLQEEEDRRAS 558
Bt_MINDY-2 509 QQDQIDQDYLMALSLQQEQQSQEINWEQIPEGISDLELAKKLQEEEDRRAS 559
Mm_MINDY-2 486 QQDQIDQDYLMALSLQQEQQSQEINWEQIPEGISDLELAKKLQEEEDRRAS 536
Rn_MINDY-2 484 QQDQIDQDYLMALSLQQEQQSQDINWEQIPEGISDLELAKKLQEEEDRRAS 534
xxDΦxLAxxLxx###x
xxDΦxLAxxLxx###x
B
MIU1 MIU2
FAM63A/
MINDY-1
MINDY
CAAX
MIU1 MIU2
FAM63B/
MINDY-2
MINDY
CAAX
C
Ub4 25% input
Halo-UBD
pulldown
Ub4: M1 K6 K11 K29 K33 K48 K63 M1 K6 K11 K29 K33 K48 K63
MINDY-1
tMIU
MINDY-2
tMIU
silver staining

Figure 2

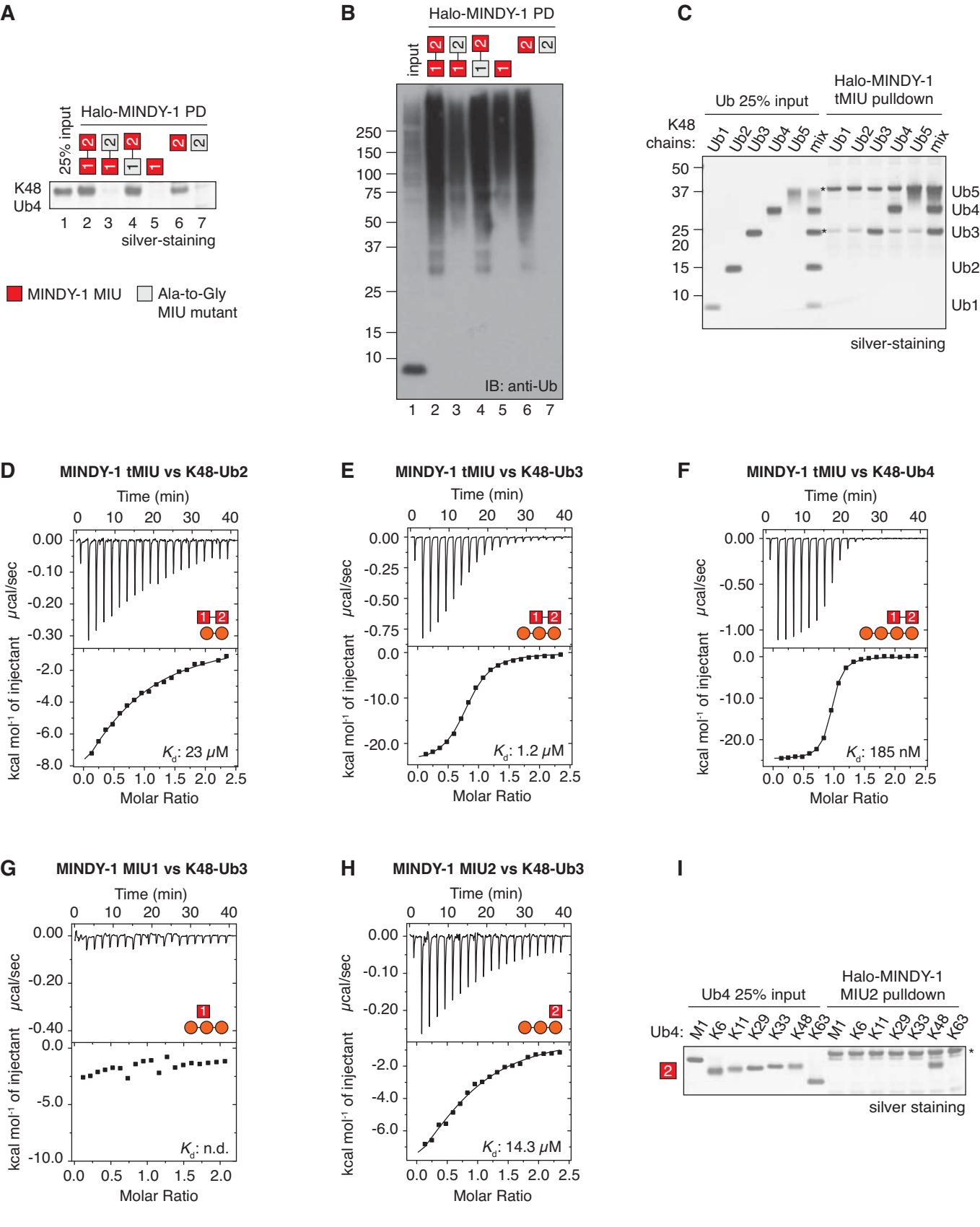
A
Halo-MINDY-1 PD
25% input
K48 Ub4
1 2 3 4 5 6 7
silver-staining
MINDY-1 MIU
Ala-to-Gly MIU mutant
B
Halo-MINDY-1 PD
input
250
150
100
75
50
37
25
15
10
IB: anti-Ub
1 2 3 4 5 6 7
C
Ub 25% input
Halo-MINDY-1 tMIU pulldown
K48 chains:
Ub1 Ub2 Ub3 Ub4 Ub5 mix Ub1 Ub2 Ub3 Ub4 Ub5 mix
50
37
25
20
15
10
Ub5
Ub4
Ub3
Ub2
Ub1
silver-staining
D
MINDY-1 tMIU vs K48-Ub2
Time (min)
µcal/sec
kcal mol-1 of injectant
Kd: 23 µM
Molar Ratio
E
MINDY-1 tMIU vs K48-Ub3
Kd: 1.2 µM
F
MINDY-1 tMIU vs K48-Ub4
Kd: 185 nM
G
MINDY-1 MIU1 vs K48-Ub3
Kd: n.d.
H
MINDY-1 MIU2 vs K48-Ub3
Kd: 14.3 µM
I
Ub4 25% input
Halo-MINDY-1 MIU2 pulldown
Ub4: M1 K6 K11 K29 K33 K48 K63 M1 K6 K11 K29 K33 K48 K63
silver staining

Figure 3

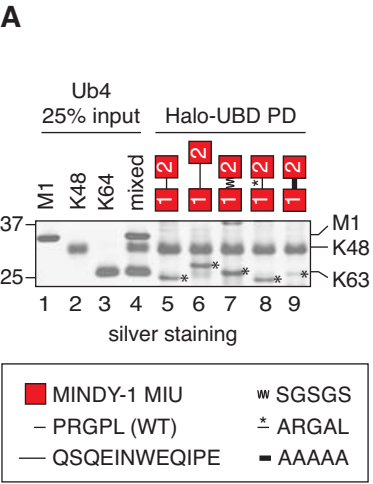
A
Ub4
25% input
Halo-UBD PD
M1
K48
K64
mixed
37
25
M1
K48
K63
1 2 3 4 5 6 7 8 9
silver staining
MINDY-1 MIU
PRGPL (WT)
QSQEINWEQIPE
SGSGS
ARGAL
AAAAA

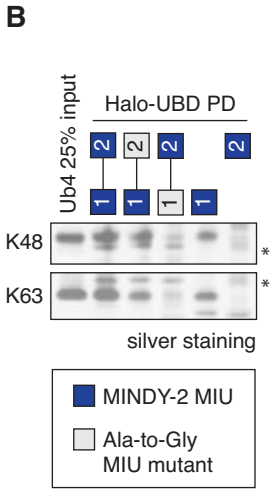
B
Ub4 25% input
Halo-UBD PD
K48
K63
silver staining
MINDY-2 MIU
Ala-to-Gly
MIU mutant

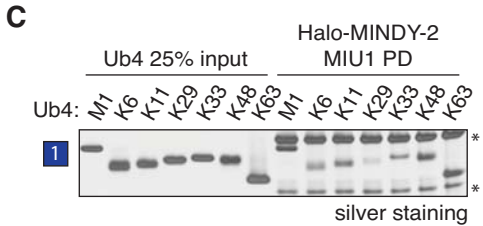
C
Ub4 25% input
Halo-MINDY-2
MIU1 PD
Ub4:
M1 K6 K11 K29 K33 K48 K63 M1 K6 K11 K29 K33 K48 K63
silver staining

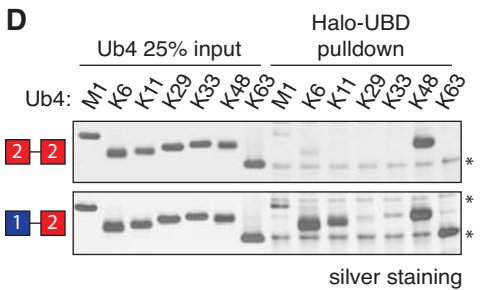
D
Ub4 25% input
Halo-UBD
pulldown
Ub4:
M1 K6 K11 K29 K33 K48 K63 M1 K6 K11 K29 K33 K48 K63
silver staining

Figure 4

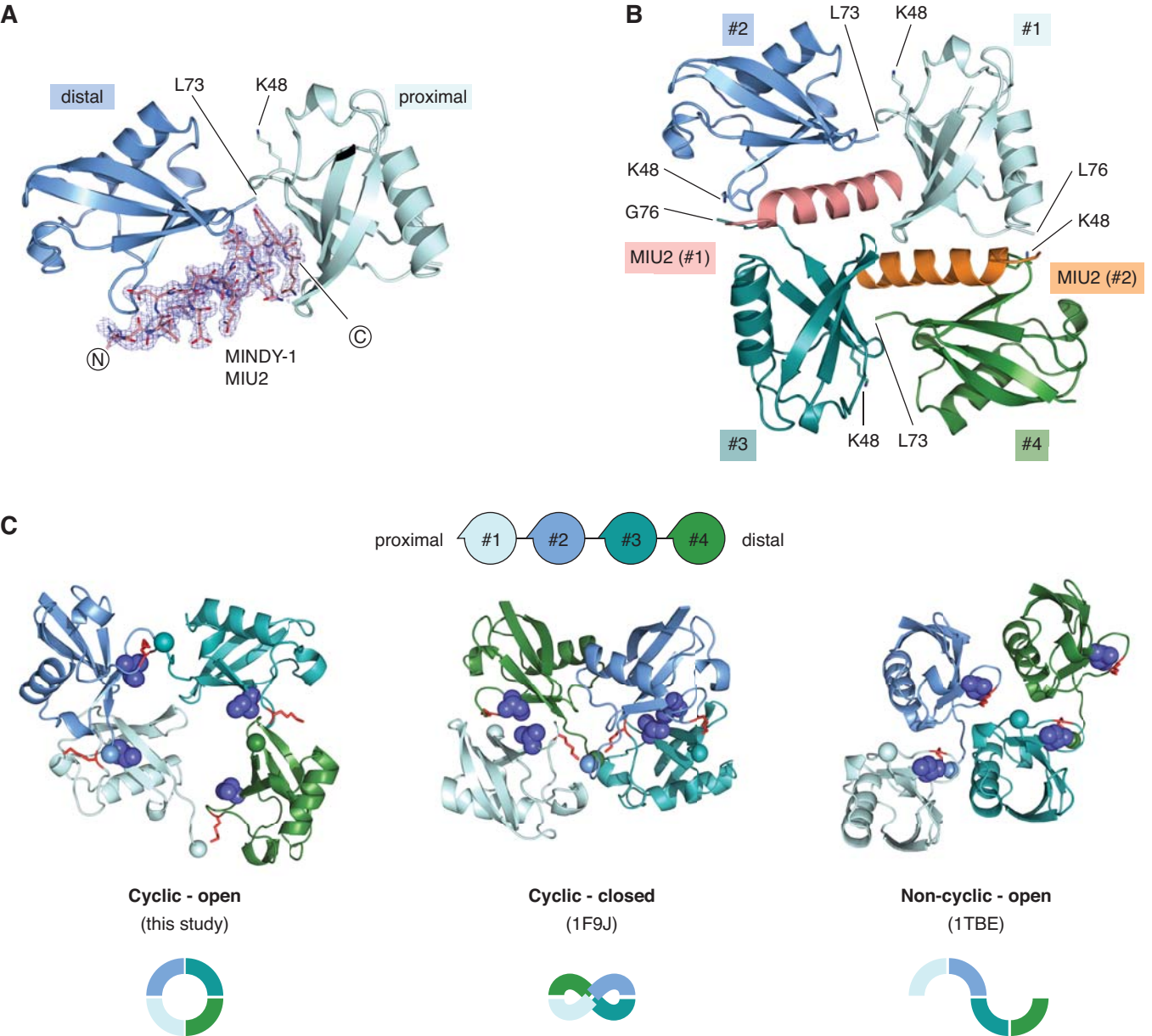
A
distal
L73
K48
proximal
N
C
MINDY-1
MIU2
B
#2
L73
K48
#1
K48
L76
G76
K48
MIU2 (#1)
MIU2 (#2)
#3
K48
L73
#4
C
proximal
#1
#2
#3
#4
distal
Cyclic - open
(this study)
Cyclic - closed
(1F9J)
Non-cyclic - open
(1TBE)

Figure 5

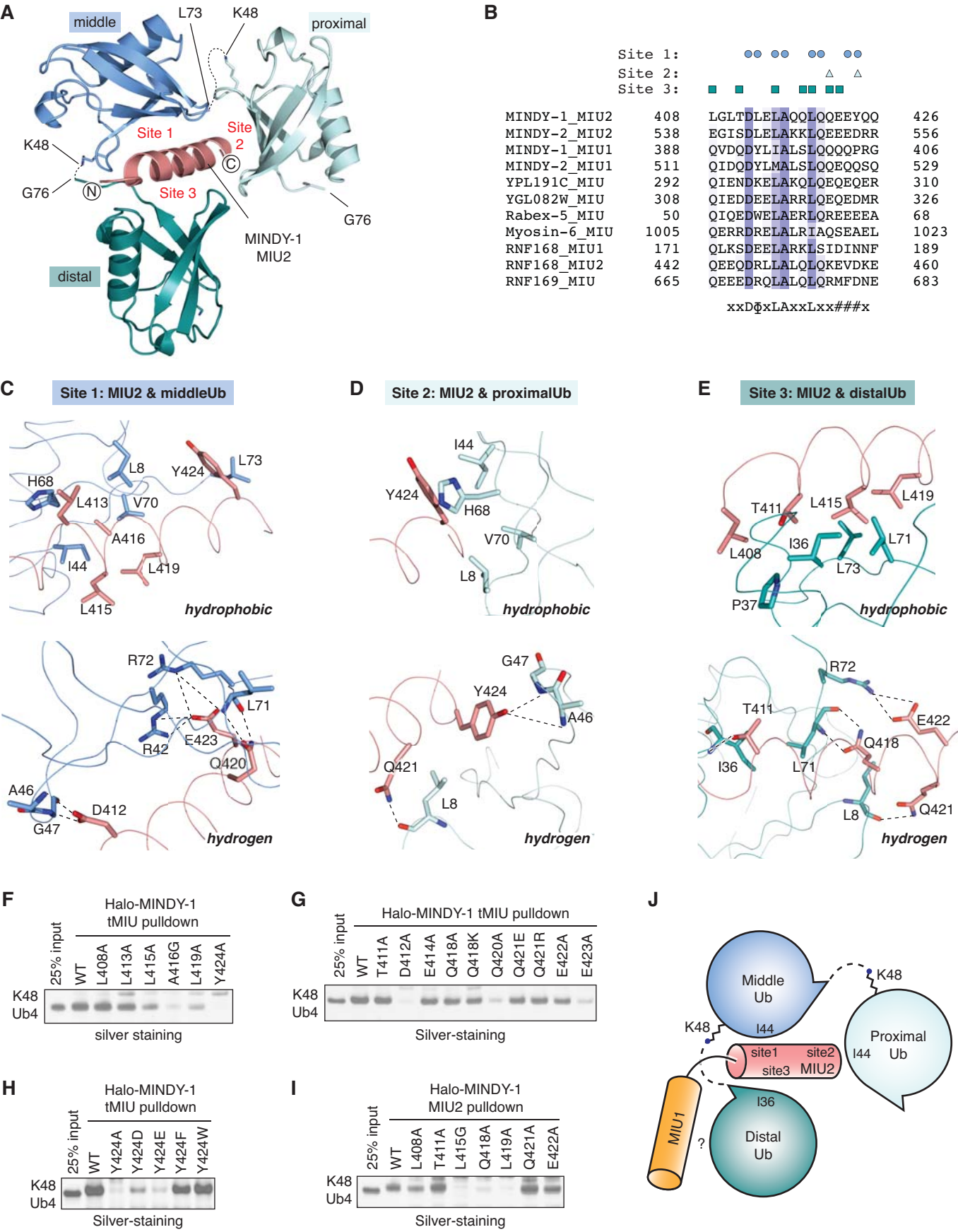
A
middle
L73
K48
proximal
Site 1
Site 2
K48
G76
Site 3
G76
MINDY-1
MIU2
distal
B
Site 1:
Site 2:
Site 3:
MINDY-1_MIU2 408 LGLTDLELAQQLQQEEYQQ 426
MINDY-2_MIU2 538 EGISDLELAKKLQEEEDRR 556
MINDY-1_MIU1 388 QVDQDYLIALSLQQQQPRG 406
MINDY-2_MIU1 511 QIDQDYLMALSLQQEQQSQ 529
YPL191C_MIU 292 QIENDKELAKQLQEQEQER 310
YGL082W_MIU 308 QIEDDEELARRLQEQEDMR 326
Rabex-5_MIU 50 QIQEDWELAERLQREEEEA 68
Myosin-6_MIU 1005 QERRDRELALRIAQSEAEL 1023
RNF168_MIU1 171 QLKSDEELARKLSIDINNF 189
RNF168_MIU2 442 QEEQDRLLALQLQKEVDKE 460
RNF169_MIU 665 QEEEDRQLALQLQRMFDNE 683
xxDΦxLAxxLxx###x
C
Site 1: MIU2 & middleUb
H68
L8
Y424
L73
L413
V70
A416
I44
L419
L415
hydrophobic
R72
L71
R42
E423
Q420
A46
D412
G47
hydrogen
D
Site 2: MIU2 & proximalUb
I44
Y424
H68
V70
L8
hydrophobic
G47
Y424
A46
Q421
L8
hydrogen
E
Site 3: MIU2 & distalUb
T411
L415
L419
L408
I36
L71
L73
P37
hydrophobic
R72
T411
E422
Q418
I36
L71
L8
Q421
hydrogen
F
Halo-MINDY-1
tMIU pulldown
25% input
WT
L408A
L413A
L415A
A416G
L419A
Y424A
K48
Ub4
silver staining
G
Halo-MINDY-1 tMIU pulldown
25% input
WT
T411A
D412A
E414A
Q418A
Q418K
Q420A
Q421E
Q421R
E422A
E423A
K48
Ub4
Silver-staining
J
Middle
Ub
K48
K48
I44
site1
site2
site3
MIU2
Proximal
Ub
I44
MIU1
I36
?
Distal
Ub
H
Halo-MINDY-1
tMIU pulldown
25% input
WT
Y424A
Y424D
Y424E
Y424F
Y424W
K48
Ub4
Silver-staining
I
Halo-MINDY-1
MIU2 pulldown
25% input
WT
L408A
T411A
L415G
Q418A
L419A
Q421A
E422A
K48
Ub4
Silver-staining

Figure EV1

A

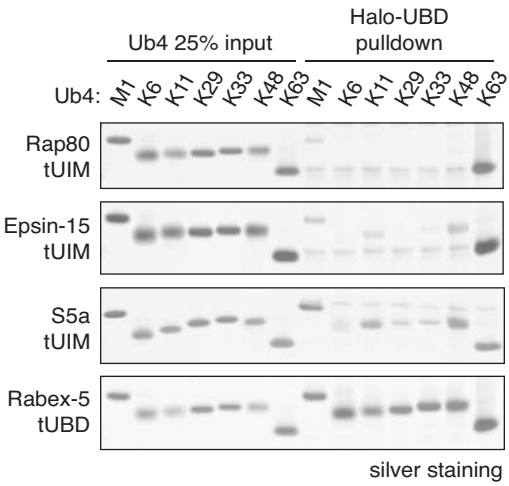

B

MINDY-1 tMIU

MIU1 (388-403)
MIU2 (406-426)
tMIU (388-426)

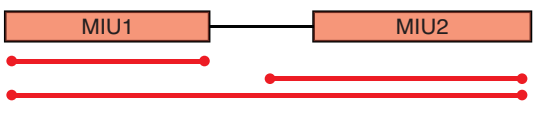


```
H_sapiens/383-431          PETQLQVDQDYLIALSLQQQQ--PRGPLGLTDLELAQQLQQEEYQQQQAAQ
P_troglodytes/431-479      PEKQLQVDQDYLIALSLQQQQ--PRGPLGLTDLELAQQLQQEEYQQQQAAQ
G_gorilla/431-479          PEKQLQVDQDYLIALSLQQQQ--PRGPLGLTDLELAQQLQQEEYQQQQAAQ
P_abelil/383-431           PEKQLQVDQDYLIALSLQQQQ--PRGTLGLTDLELAQQLQQEEYQQQQAAQ
P_macrocephalus/383-431    PEKQRQVDQDYLIALSLQQQ--PSQGTLGLSDLELAQQLQQEEYQQHQATQ
L_vexillifer/383-431       PEKQRQVDQDYLIALSLQQQ--PSQGTLGLSDLELAQQLQQEEYQQHQAAQ
P_tigris/383-430           PEQQRLVDQDYLIALSLQQQ---PQGTLGLSDLELAQQLQQEEYQQQPAVQ
U_maritimus/383-430        PEKRRQVDQDYLIALSLQQQ---PQATLGLSDLELAQQLQQEEYQQQQAVQ
B_taurus/383-433           PEKQRQVDQDYLIALSLQQQQPPPQGTSGLSDLELAQQLQQEEYQQHQAAQ
E_caballus/386-436         PEKQRQVDQDYLIALSLQQQQQQPQGTLGLSDLELAQQLQQEEYQQQQALQ
C_bacterianus/383-432      PEKQRQVDQDYLIALSLQQQQ-QPQGTLGLSDLELAQQLQQEEYQQHQAVQ
C_lupus/380-427            PKELRQVDQDYLIALSLQQQ---PQGTLGLSDLELAQRLQQEEYQQQQAVQ
F_catus/381-428            PEQQRLVDQDYLIALSLQQQ---PQGTLGLSDLELAQQLQQEEYQQQPAVQ
O_cuniculus/383-433        PEKQLQVDQDYLIALSLQQQQPAPQGTLGLSDLELAQQLQQEEYQQQQGVQ
M_musculus/383-432         PEKQLQVDQDYLIALSLQQQQ-QPQGTLGLSDLELAQQLQQEEYQQQQAVQ
R_norvegicus/397-446       PEKQLQVDQDYLIALSLQQQQ-QPQGMLGLSDLELAQQLQQEEYQQQQAVQ
M_domestica/382-430        QETQRQVDQDYMIALSLQQQQ--QQGTLGLSDLELARQLQQEEYQQQQVQP
G_gallus/383-430           PE-QSQLDQDYMMALSLQQQQ--GQGPSALSDLELARQLQQEEYQQQQQQQ
H_leucocephalus/397-445    RLQQRQVDQDYMIALSLQQQQ--GQDPSVLSDLELAHQLQQEEYHHHHHHQ
X_tropicalis/419-466       QLQQRQVDQDYMIALSLQQQ---QQGPLAMSDLELAQQLQQEEYQQQQQQQ
T_rubripes/275-322         EEQQRQIDQDYLVAVSLQQ-Q--GGAAGPLSDLELARQLQQEEYQNQQHLQ
D_rerio/436-484            QQQQMQIDQDYLVAMSLQQEQ--GEAPGPLSDLELARQLQQEEYQQPQTQQ

                           xxDΦxLAxxLxx###x        xxDΦxLAxxLxx###x
```

C

MINDY-2 tMIU

MIU1 (507-526)
MIU2 (535-559)
tMIU (507-559)

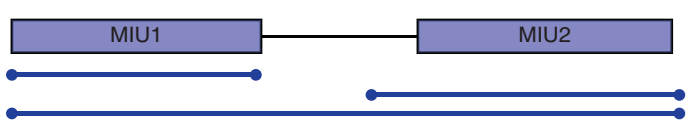


```
H_sapiens/502-562          ETVYKGQQDQIDQDYLMALSLQQEQQSQEINWEQIPEGISDLELAKKLQEEEDRRASQYYQ
P_troglodytes/502-562      ETVYKGQQDQIDQDYLMALSLQQEQQSQEINWEQIPEGISDLELAKKLQEEEDRRASQYYQ
P_abelii/502-562           ETVYKGQQDQIDQDYLMALSLQQEQQSQEINWEQIPEGISDLELAKKLQEEEDRRASQYYQ
B_taurus/503-563           ETVYRGQQDQIDQDYLMALSLQQEQQSQEINWEQIPEGISDLELAKKLQEEEDRRASQYYQ
O_aries/468-528            ETVYRGQQDQIDQDYLMALSLQQEQQSQEINWEQIPEGISDLELAKKLQEEEDRRASQYYQ
F_catus/508-568            ETVYRGQQDQIDQDYLMALSLQQEQQSQEINWEQIPEGISDLELAKKLQEEEDRRASQYYQ
O_cuniculus/503-563        ETVYKGQQDQIDQDYLMALSLQQEQQNQEINWEQIPEGISDLELAKKLQEEEDRRASQYYQ
M_musculus/480-540         ETVYKGQQDQIDQDYLMALSLQQEQQSQEINWEQIPEGISDLELAKKLQEEEDRRASQYYQ
R_norvegicus/478-538       ETVYKGQQDQIDQDYLMALSLQQEQQSQDINWEQIPEGISDLELAKKLQEEEDRRASQYYQ
D_rerio/495-555            ETVYRGQQDQIDQDYLMALSLQQEQQASDLGWEQIPEGISDLELAKKLQEEEDRRASQYYQ

                           xxDΦxLAxxLxx###x        xxDΦxLAxxLxx###x
```

Figure EV2

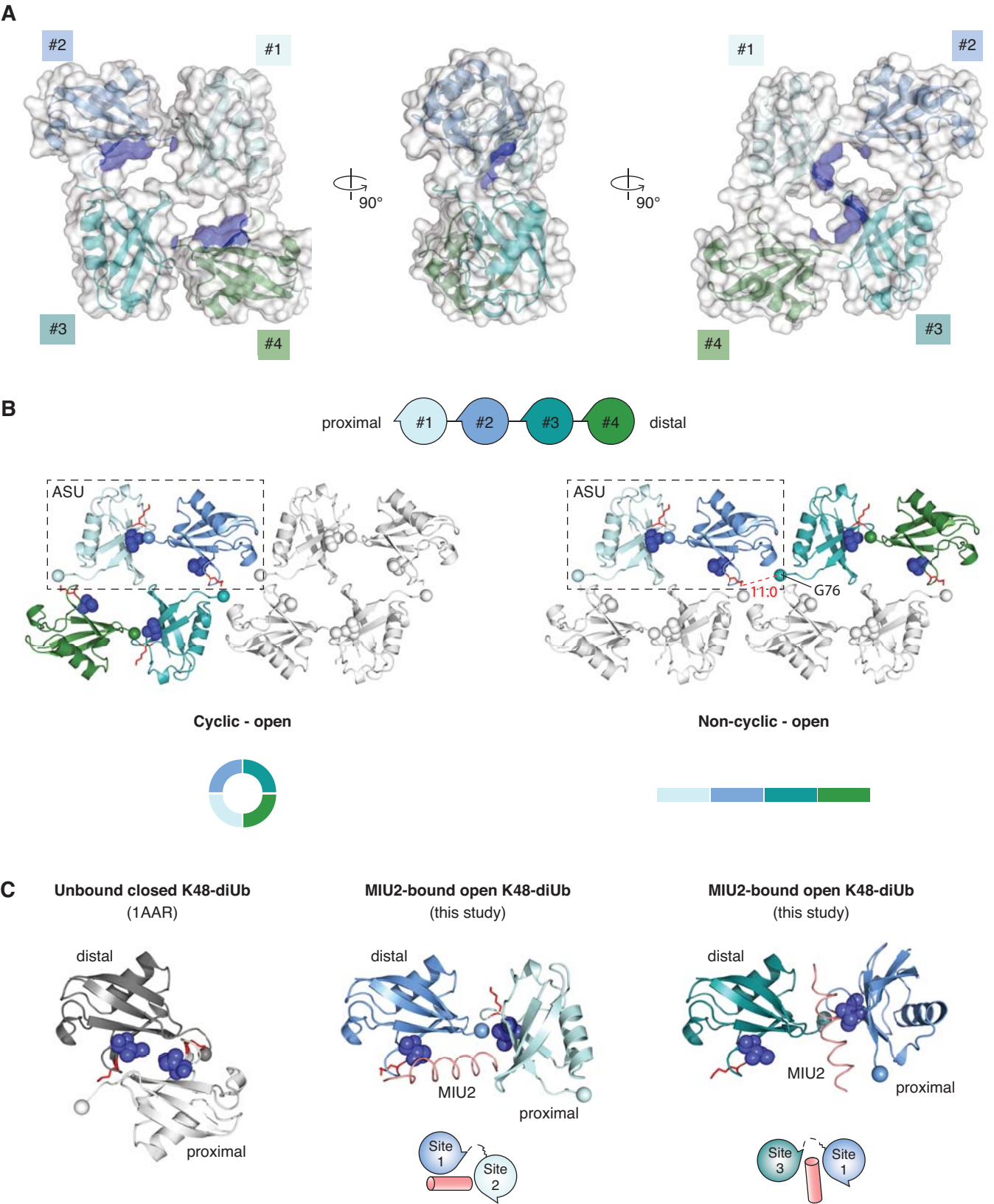
A
#2
#1
#3
#4
90°
90°
#1
#2
#4
#3
B
proximal
#1
#2
#3
#4
distal
ASU
ASU
11.0
G76
Cyclic - open
Non-cyclic - open
C
Unbound closed K48-diUb
(1AAR)
MIU2-bound open K48-diUb
(this study)
MIU2-bound open K48-diUb
(this study)
distal
proximal
distal
MIU2
proximal
distal
MIU2
proximal
Site 1
Site 2
Site 3
Site 1

Figure EV3

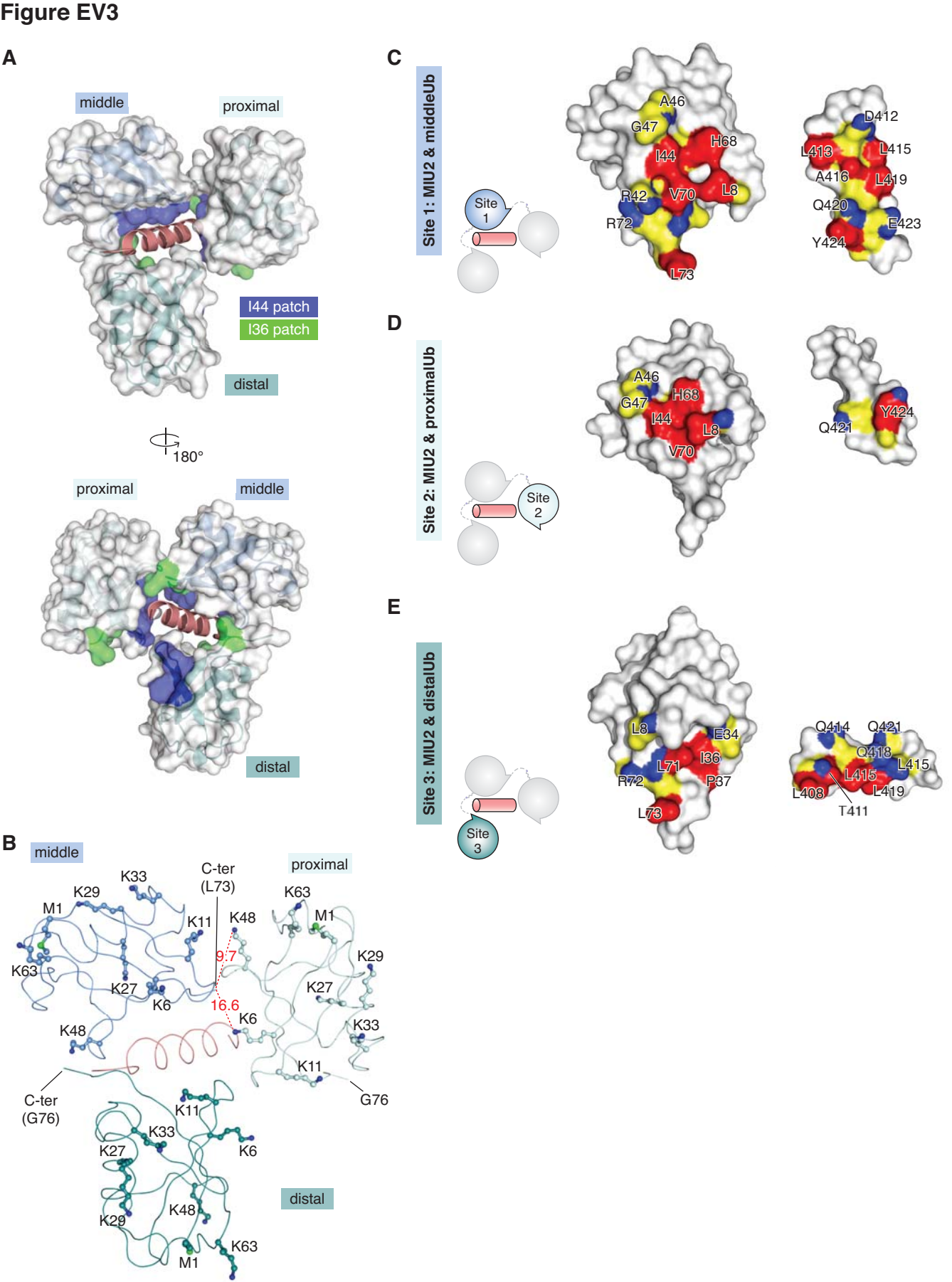
A
middle
proximal
I44 patch
I36 patch
distal
180°
proximal
middle
distal
B
middle
proximal
distal
M1
K29
K33
C-ter
(L73)
K11
K48
K63
9.7
K27
K6
16.6
K6
K48
C-ter
(G76)
K11
K33
K27
K6
K29
K48
K63
M1
K63
M1
K29
K27
K33
K11
G76
C
Site 1: MIU2 & middleUb
Site
1
A46
G47
H68
I44
R42
V70
L8
R72
L73
D412
L413
L415
A416
L419
Q420
E423
Y424
D
Site 2: MIU2 & proximalUb
Site
2
A46
H68
G47
I44
L8
V70
Y424
Q421
E
Site 3: MIU2 & distalUb
Site
3
L8
E34
I36
L71
R72
P37
L73
Q414
Q421
Q418
L415
L415
L408
L419
T411

Figure EV4

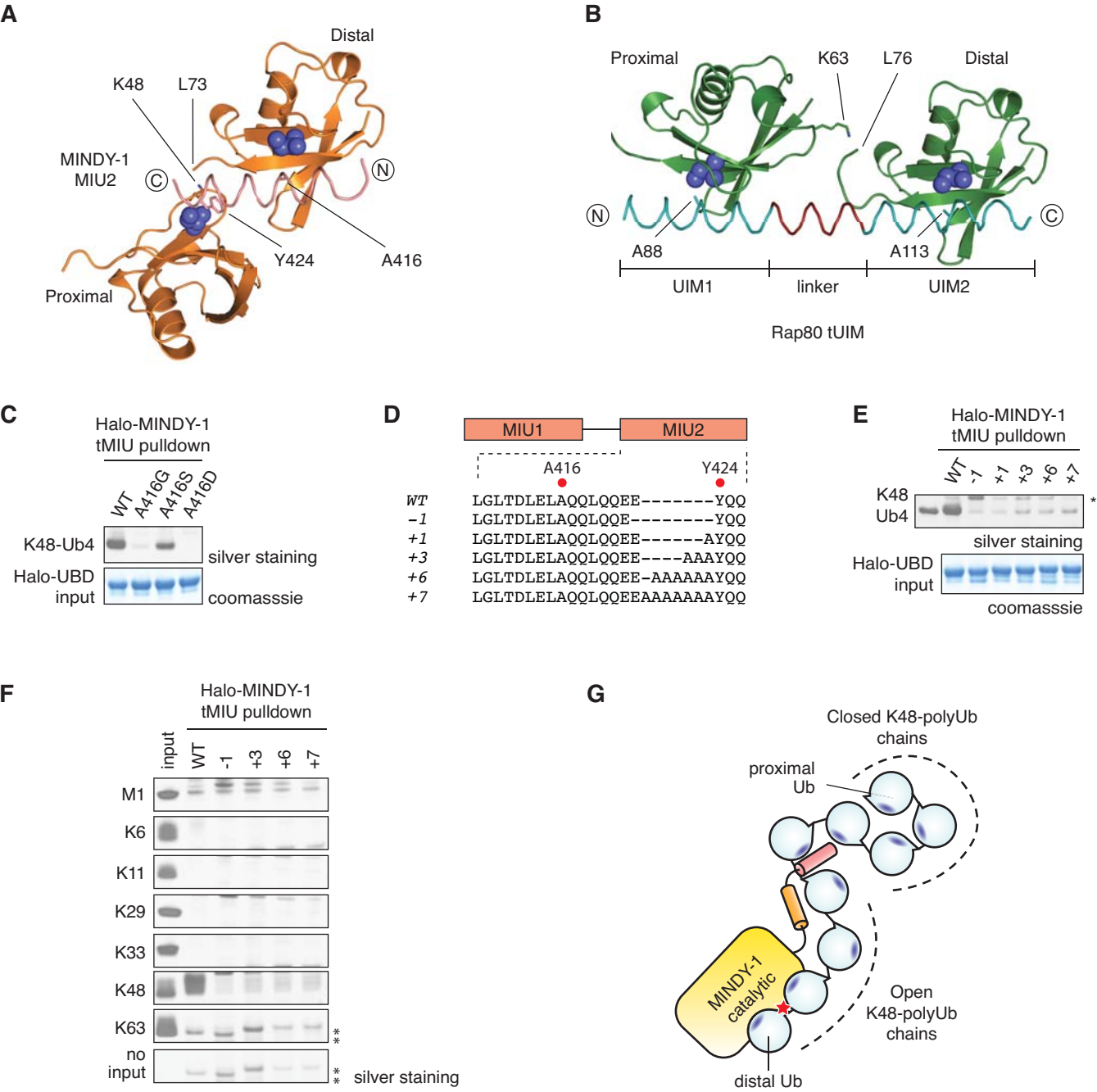
A
Distal
K48
L73
MINDY-1
MIU2
C
N
Y424
A416
Proximal
B
Proximal
K63
L76
Distal
N
C
A88
A113
UIM1
linker
UIM2
Rap80 tUIM
C
Halo-MINDY-1
tMIU pulldown
WT
A416G
A416S
A416D
K48-Ub4
silver staining
Halo-UBD
input
coomasssie
D
MIU1
MIU2
A416
Y424
WT LGLTDLELAQQLQQEE-------YQQ
−1 LGLTDLELAQQLQQE--------YQQ
+1 LGLTDLELAQQLQQEE------AYQQ
+3 LGLTDLELAQQLQQEE----AAAYQQ
+6 LGLTDLELAQQLQQEE-AAAAAAYQQ
+7 LGLTDLELAQQLQQEEAAAAAAAYQQ
E
Halo-MINDY-1
tMIU pulldown
WT
-1
+1
+3
+6
+7
K48
Ub4
*
silver staining
Halo-UBD
input
coomasssie
F
Halo-MINDY-1
tMIU pulldown
input
WT
-1
+3
+6
+7
M1
K6
K11
K29
K33
K48
K63
**
no
input
**
silver staining
G
Closed K48-polyUb
chains
proximal
Ub
MINDY-1
catalytic
Open
K48-polyUb
chains
distal Ub

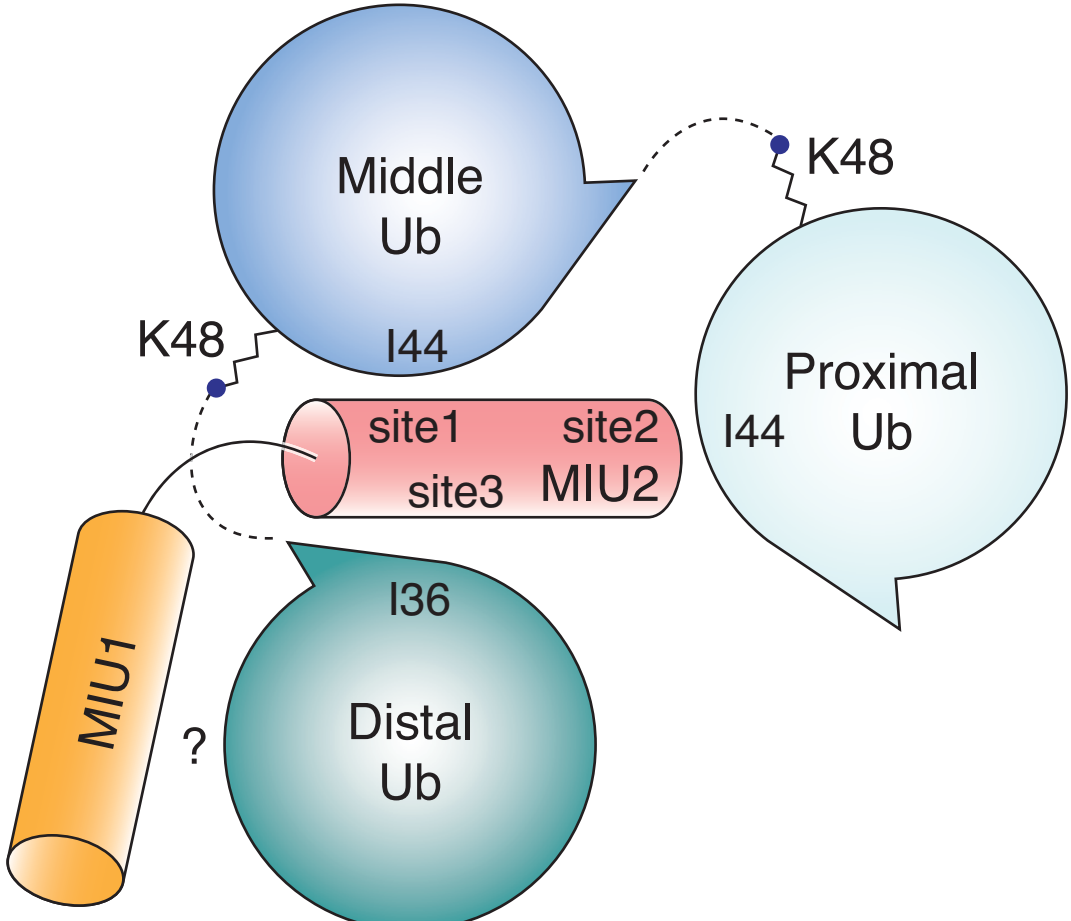
Middle
Ub
K48
I44
K48
Proximal
I44
Ub
site1
site2
site3
MIU2
MIU1
?
I36
Distal
Ub

A single MIU motif of MINDY-1 recognizes K48-linked polyubiquitin chains

Yosua Adi Kristariyanto, Syed Arif Abdul Rehman, Simone Weidlich, Axel Knebel and Yogesh Kulathu

MRC Protein Phosphorylation and Ubiquitylation Unit, College of Life Sciences, University of Dundee, Dow Street, Dundee DD1 5EH, UK

Appendix

Table of Contents

Appendix Table S1: Data collection and refinement statistics

	MINDY-1 tMIU:K48-diUb
Wavelength (Å)	0.96769
Beamline	ID30A
Resolution range (Å)	48.87-2.05 (2.05-2.11)
Space group	$I4_1$
Unit cell dimensions	55.14 55.14 105.51 90.00 90.00 90.00
Total reflections	65512 (5060)
Unique reflections	9899 (765)
Multiplicity	6.6 (6.6)
Completeness (%)	100 (100)
$I/\sigma I$	19.4 (2.9)
R-merge	0.043 (0.544)
$CC_{1/2}$	0.999 (0.818)
R_{work}	0.1826
R_{free}	0.2234
Average *B*-factor	37.0
macromolecules	1335
water	3
RMS (bonds)	0.010
RMS (angles)	1.441
Ramachandran favored (%)	100
Ramachandran allowed (%)	0
Ramachandran outliers (%)	0

Appendix Table S2: cDNA construct used in the study

All constructs were made in pGEX6P backbone. All proteins are Halo-tagged, except those indicated with asterisks, which are untagged. Sequences were retrieved from Uniprot with accession codes of Q8N5J2-1 (MINDY-1/FAM63A), Q8NBR6-1 (MINDY-2/FAM63B), Q96RL1-1 (Rap80), P42566-1 (Epsin-15), P55036-1 (S5a) and Q9UJ41-2 (Rabex-5).

Protein	DU number	Construct Boundaries
MINDY-1 tMIU	47443	388-426
MINDY-1 tMIU A416G	47712	388-426
MINDY-1 tMIU A396G	47985	388-426
MINDY-1 MIU1	55039	388-403
MINDY-1 MIU2	47422	406-426
MINDY-1 MIU2 A416G	47512	406-426
MINDY-1 tMIU (linker QSQEINWEQIPE)	48000	388-403 + linker + 409-426
MINDY-1 tMIU (linker SGSGS)	55001	388-403 + linker + 409-426
MINDY-1 tMIU (linker ARGAL)	55020	388-403 + linker + 409-426
MINDY-1 tMIU (linker AAAAA)	55044	388-403 + linker + 409-426
MINDY-1 tMIU L408A	55225	388-426
MINDY-1 tMIU T411A	55241	388-426
MINDY-1 tMIU D412A	55259	388-426
MINDY-1 tMIU L413A	47703	388-426
MINDY-1 tMIU E414A	55226	388-426
MINDY-1 tMIU L415A	47711	388-426
MINDY-1 tMIU A416G	47712	388-426
MINDY-1 tMIU A416S	47762	388-426
MINDY-1 tMIU A416D	55396	388-426
MINDY-1 tMIU Q418A	55227	388-426
MINDY-1 tMIU Q418K	55358	388-426
MINDY-1 tMIU L419A	47708	388-426
MINDY-1 tMIU Q420A	55242	388-426
MINDY-1 tMIU Q421E	47827	388-426
MINDY-1 tMIU Q421R	47828	388-426
MINDY-1 tMIU E422A	55395	388-426
MINDY-1 tMIU E423A	55243	388-426
MINDY-1 tMIU Y424A	47721	388-426
MINDY-1 tMIU Y424D	47767	388-426
MINDY-1 tMIU Y424E	47759	388-426
MINDY-1 tMIU Y424F	47760	388-426

MINDY-1 tMIU Y424W	47768	388-426
MINDY-1 MIU2 L408A	55463	406-426
MINDY-1 MIU2 T411A	28668	406-426
MINDY-1 MIU2 L415G	47513	406-426
MINDY-1 MIU2 Q418A	55428	406-426
MINDY-1 MIU2 Q421A	55429	406-426
MINDY-1 MIU2 E422A	55430	406-426
MINDY-1 MIU2 L419A	47583	406-426
MINDY-1 tMIU*	49555	388-426
MINDY-1 MIU1*	47865	386-406
MINDY-1 MIU2*	47848	406-426
MINDY-1 tMIU (-1)	55221	388-426 (Δ423)
MINDY-1 tMIU (+1)	55295	388-426 (1xA in between 423&424)
MINDY-1 tMIU (+3)	55222	388-426 (2xA in between 423&424)
MINDY-1 tMIU (+6)	55223	388-426 (6xA in between 423&424)
MINDY-1 tMIU (+7)	55224	388-426 (7xA in between 423&424)
MINDY-2 tMIU	47515	507-559
MINDY-2 tMIU A546G	47758	507-559
MINDY-2 tMIU A519G	55074	507-559
MINDY-2 MIU1	55019	507-526
MINDY-2 MIU2	47542	535-559
MINDY-1 MIU2 + MINDY-1 MIU2 (linker PRGPL)	55043	409-426 + linker + 409-426
MINDY-2 MIU1 + MINDY-1 MIU2 (linker PRGPL)	55040	507-526 + linker + 409-427
Rap80 tUIM	55032	78-125
Epsin-15 tUIM	49822	851-895
S5a tUIM	49625	196-309
Rabex-5 tUIM	55021	13-73